

MIT Open Access Articles

The Quantum Theory of Optical Communications

The MIT Faculty has made this article openly available. **Please share** how this access benefits you. Your story matters.

Citation: Shapiro, J.H. "The Quantum Theory of Optical Communications." IEEE Journal of Selected Topics in Quantum Electronics 15.6 (2009): 1547–1569. © Copyright 2009 IEEE

As Published: <http://dx.doi.org/10.1109/JSTQE.2009.2024959>

Publisher: Institute of Electrical and Electronics Engineers (IEEE)

Persistent URL: <http://hdl.handle.net/1721.1/73495>

Version: Final published version: final published article, as it appeared in a journal, conference proceedings, or other formally published context

Terms of Use: Article is made available in accordance with the publisher's policy and may be subject to US copyright law. Please refer to the publisher's site for terms of use.



The Quantum Theory of Optical Communications

Jeffrey H. Shapiro, *Fellow, IEEE*

(Invited Paper)

Abstract—Communication theory applied to lightwave channels is ordinarily carried out using the semiclassical theory of photodetection. Recent development of nonclassical light sources—whose photodetection statistics require the use of quantum theory—plus increasing interest in optics-based approaches to quantum information processing necessitates a thorough understanding of the similarities and distinctions between the semiclassical and quantum theories of optical communications. This paper is addressed to that need, focusing, for convenience, on the free-space communication channel using Gaussian states of light. The quantum version of the Huygens–Fresnel diffraction integral is reviewed, along with the semiclassical and quantum theories of direct, homodyne, and heterodyne detection. Maximally entangled Gaussian state light is used, in conjunction with quantum photodetection theory, to explain the nonclassical effects seen in Hong–Ou–Mandel interferometry and violation of the Clauser–Horne–Shimony–Holt form of Bell’s inequality. The classical information capacities of several bosonic channels are reviewed, and shown to exceed what can be achieved using conventional optical receivers.

Index Terms—Optical communication, optical diffraction, photon beams, quantum theory.

I. INTRODUCTION

BROADBAND fiber-optic communication is arguably the key enabler of the Internet age. Lasercom satellite cross-links promise vast bandwidth increases for networks in the sky [1]–[3]. Wireless optical links, which operate over line-of-sight terrestrial paths, offer high-data-rate communications in applications for which fiber connectivity is unavailable or unaffordable [4], [5]. Communication system design and performance analysis for these classical information transmission links are usually accomplished semiclassically. In this approach, lightwaves are treated as classical electromagnetic fields, which may carry unwanted fluctuations in addition to the desired information-bearing modulation, and the fundamental noise encountered in photodetection is the shot noise associated with the discreteness of the electron charge (see, e.g., [6] and [7]). Despite the success of these semiclassical treatments, it must be remembered that electromagnetic waves are quantized, and that high-sensitivity photodetection systems have long been limited by noise of quantum-mechanical origin. It would, therefore, seem that high-performance optical communication systems should be analyzed and designed within a fully quantum

mechanical framework. That such is *not* necessary, in most situations, is due to the exact quantitative agreement between the semiclassical and quantum theories for direct detection, homodyne detection, and heterodyne detection when the illuminating light beam is in what is known as a classical state [8]. Indeed, as these three photodetection modalities represent the primary schemes for optical reception, and classical light states are produced by natural illumination, LEDs, and lasers, it is only in specialized circumstances that quantum photodetection must be employed, e.g., in experiments involving nonclassical light states such as single photons [9], squeezed states [10], or entangled states [11], [12].

Nonclassical states are now receiving considerable attention for their roles in *quantum* information applications: qubits encoded in single photons [13], continuous-variable quantum information encoded in squeezed states [14], and entanglement used to effect quantum-state teleportation [15], [16]. The fully quantum analyses of such systems are frequently presented in terms of photon annihilation operators for the one or two relevant field modes. As such, their resemblance to semiclassical treatments of classical information transmission via lightwaves—in which temporal and even spatiotemporal characteristics are of explicit importance—is minimal. This disconnect needs to be bridged for two reasons. First, analyses of optics-based quantum communication and information processors must confront the full spatiotemporal behavior of their quantized fields to properly assess their performance (see [17] for a temporal-mode example). Second, recent theoretical studies have shown that the classical information capacities of bosonic channels, of which lightwave channels are the prime examples, *exceed* what can be realized with conventional, i.e., direct, homodyne, or heterodyne, receivers [18]. Thus, those involved in classical information transmission *and* those working on quantum information transmission should understand both the semiclassical and quantum theories of optical communication. This tutorial paper is addressed to that need, focusing, for convenience, on the free-space (vacuum propagation) channel using Gaussian states of light.

The remainder of this paper is organized as follows. In Section II, we begin with a review of the standard approach to quantizing the electromagnetic field [19]. Then, we show how this formulation can be reduced to the quantum version of the scalar Fresnel diffraction formula for line-of-sight free-space communication using a single polarization in the quasinonochromatic, paraxial regime [20]. By performing a normal-mode decomposition [21] for quantum diffraction between a transmitter pupil and a receiver pupil, we will obtain the near-field and far-field operating regimes for this channel.

We devote Section III to Gaussian states of light [22], including coherent states, thermal states, and squeezed states

Manuscript received March 5, 2009; revised May 5, 2009. First published August 25, 2009; current version published December 3, 2009. Preparation of this paper was supported by the Office of Naval Research Basic Research Challenge Program, the DARPA Quantum Sensors Program, and the W. M. Keck Foundation Center for Quantum Information.

The author is with the Research Laboratory of Electronics, Massachusetts Institute of Technology, Cambridge, MA 02139 USA (e-mail: jhs@mit.edu).

Color versions of one or more of the figures in this paper are available online at <http://ieeexplore.ieee.org>.

Digital Object Identifier 10.1109/JSTQE.2009.2024959

of a single field operator, and maximally entangled Gaussian states of two field operators. The single-operator states are important because coherent states yield the classical limit of noiseless electromagnetic radiation [23], squeezed states play an essential role in several schemes for subshot-noise precision measurements [24], [25], and quantum Gaussian noise (thermal-state light) appears in models for several important optical communication channels [26]. The two-operator states can be produced by spontaneous parametric downconversion (SPDC) [27], and figure prominently in heralded generation of single photons [28], [29] and the production of polarization singlets for use in qubit teleportation [12], [15].

In Section IV, we present the semiclassical and quantum theories of photodetection. Here, we will describe the statistical characterizations of direct, homodyne, and heterodyne detection, and point to their equivalence when the illumination is in a coherent state or a random mixture of coherent states [8]. We will also use the maximally entangled Gaussian state produced by SPDC to illustrate the nonclassical fourth-order interference seen in Hong–Ou–Mandel (HOM) interferometry [30], and the violation of the Clauser–Horne–Shimony–Holt (CHSH) form of Bell’s inequality [31].

Our final topic, which is the subject of Section V, will be the classical information capacities of bosonic channels [18], [32], [33]. Here, we shall review recent results for the pure-loss and thermal-noise channels, comparing the capacity that is achieved in full quantum theory with what is predicted for structured reception using direct, homodyne, or heterodyne detection. Throughout this paper, we shall minimize derivation details, focusing instead upon results and their interpretations. The interested reader may consult the references for more information.

II. ELECTROMAGNETIC FIELD QUANTIZATION AND PROPAGATION

Textbook treatments of electromagnetic field quantization approach that task as an initial value problem, i.e., the electromagnetic field within a specified region of 3-D space is quantized at time $t = 0$ and then evolved forward in time [19]. In contrast, the classical field calculations used in a semiclassical analysis of a free-space optical communication link take the form of a boundary-value problem: The electromagnetic field within the transmitter’s exit pupil during the time interval within which transmission will occur is specified, and the field that results within the receiver’s entrance pupil is calculated via diffraction theory. In this section, we review standard initial-value field quantization and reduce it to a quantum version of Fresnel diffraction within the quasi-monochromatic, paraxial operating regime [20]. We also introduce the spatial-mode decomposition for that diffraction problem.

A. Quantization as an Initial Value Problem

Starting from Maxwell’s equations for a classical electromagnetic field propagating in a source-free region of free space, using separation of variables for the field’s spatial and temporal dependence, and imposing periodic boundary conditions on an $L \times L \times L$ unit cube lead to the following expansion for the

electric field:

$$\mathbf{E}(\mathbf{r}, t) = \mathbf{E}^{(+)}(\mathbf{r}, t) + \mathbf{E}^{(-)}(\mathbf{r}, t) \quad (1)$$

with the positive-frequency field $\mathbf{E}^{(+)}$ satisfying

$$\mathbf{E}^{(+)}(\mathbf{r}, t) = \sum_{\mathbf{m}, \sigma} j \sqrt{\frac{\hbar \omega_{\mathbf{m}}}{2\epsilon_0 L^3}} a_{\mathbf{m}, \sigma} e^{-j(\omega_{\mathbf{m}} t - \mathbf{k}_{\mathbf{m}} \cdot \mathbf{r})} \mathbf{e}_{\mathbf{m}, \sigma} \quad (2)$$

and the negative-frequency field $\mathbf{E}^{(-)}$ being its complex conjugate. This is a plane-wave modal decomposition in which the (\mathbf{m}, σ) mode, where \mathbf{m} is a 3-D vector with integer components and $\sigma = 0$ or 1 , has wave vector $\mathbf{k}_{\mathbf{m}} = (2\pi m_x/L, 2\pi m_y/L, 2\pi m_z/L)$, frequency $\omega_{\mathbf{m}} = c|\mathbf{k}_{\mathbf{m}}|$, and polarization specified by the unit vector $\mathbf{e}_{\mathbf{m}, \sigma}$ obeying the transversality conditions $\mathbf{e}_{\mathbf{m}, \sigma} \cdot \mathbf{k}_{\mathbf{m}} = 0$, and $\mathbf{e}_{\mathbf{m}, 0} \cdot \mathbf{e}_{\mathbf{m}, 1} = 0$. Its temporal dependence is simple harmonic motion $a_{\mathbf{m}, \sigma} e^{-j\omega_{\mathbf{m}} t}$, so that the initial-time ($t = 0$) phasor $a_{\mathbf{m}, \sigma}$ completely characterizes the amplitude and phase behavior of the mode throughout the unit cube. To extend this plane-wave decomposition to an unbounded region, we let $L \rightarrow \infty$, thus obtaining

$$\begin{aligned} \mathbf{E}^{(+)}(\mathbf{r}, t) &= j \sqrt{\frac{\hbar}{2\epsilon_0}} \\ &\times \sum_{\sigma} \int \frac{d^3 \mathbf{k}}{(2\pi)^3} \sqrt{\omega_{\mathbf{k}}} A(\mathbf{k}, \sigma) e^{-j(\omega_{\mathbf{k}} t - \mathbf{k} \cdot \mathbf{r})} \mathbf{e}_{\mathbf{k}, \sigma} \end{aligned} \quad (3)$$

for the positive-frequency electric field.

At this point, field quantization is carried out by treating each plane-wave mode’s temporal behavior as a quantum harmonic oscillator, so that electric fields become electric field operators. For the finite-sized unit cube, we have

$$\hat{\mathbf{E}}(\mathbf{r}, t) = \hat{\mathbf{E}}^{(+)}(\mathbf{r}, t) + \hat{\mathbf{E}}^{(-)}(\mathbf{r}, t) \quad (4)$$

with the positive-frequency field operator being

$$\hat{\mathbf{E}}^{(+)}(\mathbf{r}, t) = \sum_{\mathbf{m}, \sigma} j \sqrt{\frac{\hbar \omega_{\mathbf{m}}}{2\epsilon_0 L^3}} \hat{a}_{\mathbf{m}, \sigma} e^{-j(\omega_{\mathbf{m}} t - \mathbf{k}_{\mathbf{m}} \cdot \mathbf{r})} \mathbf{e}_{\mathbf{m}, \sigma} \quad (5)$$

and the negative-frequency field $\hat{\mathbf{E}}^{(-)}$ being its adjoint. The phasor $a_{\mathbf{m}, \sigma}$ appearing in (2) for the classical positive-frequency field has now become the photon annihilation operator $\hat{a}_{\mathbf{m}, \sigma}$, whose adjoint, $\hat{a}_{\mathbf{m}, \sigma}^\dagger$, is the photon creation operator appearing in the negative-frequency field operator. The modal annihilation and creation operators have the canonical commutation relations

$$[\hat{a}_{\mathbf{m}, \sigma}, \hat{a}_{\mathbf{m}', \sigma'}] = 0 \quad (6)$$

$$[\hat{a}_{\mathbf{m}, \sigma}, \hat{a}_{\mathbf{m}', \sigma'}^\dagger] = \delta_{\mathbf{m} \mathbf{m}'} \delta_{\sigma \sigma'}. \quad (7)$$

In the limit $L \rightarrow \infty$, we get

$$\begin{aligned} \hat{\mathbf{E}}^{(+)}(\mathbf{r}, t) &= j \sqrt{\frac{\hbar}{2\epsilon_0}} \\ &\times \sum_{\sigma} \int \frac{d^3 \mathbf{k}}{(2\pi)^3} \sqrt{\omega_{\mathbf{k}}} \hat{A}(\mathbf{k}, \sigma) e^{-j(\omega_{\mathbf{k}} t - \mathbf{k} \cdot \mathbf{r})} \mathbf{e}_{\mathbf{k}, \sigma} \end{aligned} \quad (8)$$

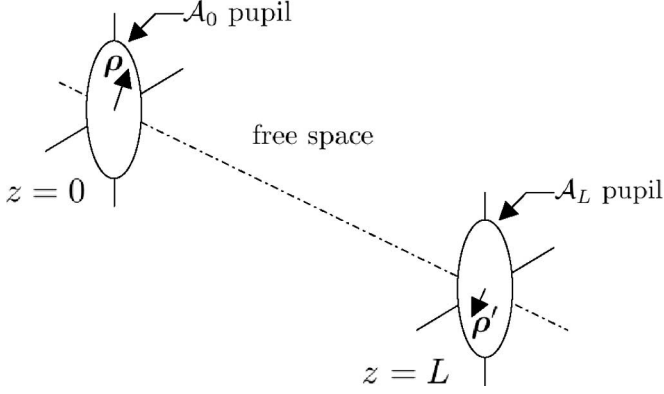


Fig. 1. Line-of-sight free-space propagation geometry.

for the positive-frequency electric field operator, where $\omega_{\mathbf{k}} = c|\mathbf{k}|$, with the canonical commutation relations

$$[\hat{A}(\mathbf{k}, \sigma), \hat{A}(\mathbf{k}', \sigma')] = 0 \quad (9)$$

$$[\hat{A}(\mathbf{k}, \sigma), \hat{A}^\dagger(\mathbf{k}', \sigma')] = (2\pi)^3 \delta(\mathbf{k} - \mathbf{k}') \delta_{\sigma\sigma'}. \quad (10)$$

The state of the field at the initial time $t = 0$ is now specified by the joint density operator at that time for the plane-wave modes associated with $\{\hat{A}(\mathbf{k}, \sigma)\}$. The field state at any later time can then be found, in principle, from this initial-time density operator and (8).

B. Quantum Diffraction Theory

Fig. 1 shows the propagation geometry for a line-of-sight free-space optical communication link. The transmitter emits an information-bearing quantized optical field through its $z = 0$ plane exit pupil \mathcal{A}_0 , and the receiver makes a quantum measurement on the light that has passed through its $z = L$ plane entrance pupil \mathcal{A}_L . The transmitter controls the state of the field in the \mathcal{A}_0 pupil, and the receiver's measurement statistics are determined by the state of the field in the \mathcal{A}_L pupil. In principle, the initial-value approach to field quantization allows the relationship between the transmitter's output state and the receiver's input state to be determined, but, in practice, it is extremely ill-matched to the task. The Fig. 1 setup begs out for the quantum version of classical diffraction theory, namely, a boundary-value approach in which the field specified in the transmitter's exit pupil is propagated through space to the receiver's entrance pupil.

To obtain the desired quantum theory of diffraction, we start from the positive-frequency electric field operator specified in (8). It is appropriate to assume in Fig. 1 that the transmitter only excites, and the receiver only measures $+z$ -propagating modes, whose positive-frequency field operator is

$$\begin{aligned} \hat{\mathbf{E}}_{(+)}^{(+)}(\mathbf{r}, t) &= j\sqrt{\frac{\hbar}{2\epsilon_0}} \\ &\times \sum_{\sigma} \int_{k_z > 0} \frac{d^3\mathbf{k}}{(2\pi)^3} \sqrt{\omega_{\mathbf{k}}} \hat{A}(\mathbf{k}, \sigma) e^{-j(\omega_{\mathbf{k}}t - \mathbf{k} \cdot \mathbf{r})} \mathbf{e}_{\mathbf{k}, \sigma}. \end{aligned} \quad (11)$$

Using the free-space dispersion relation $\omega_{\mathbf{k}} = c|\mathbf{k}|$, we can rewrite the preceding expression as follows:

$$\begin{aligned} \hat{\mathbf{E}}_{(+)}^{(+)}(\mathbf{r}, t) &= j\sqrt{\frac{\hbar}{2\epsilon_0}} \sum_{\sigma} \\ &\times \int_0^\infty \frac{d\omega}{2\pi c} \int_{|\mathbf{k}_T| < \omega/c} \frac{d^2\mathbf{k}_T}{(2\pi)^2} \sqrt{\frac{\omega^3}{\omega^2 - c^2|\mathbf{k}_T|^2}} \hat{A}(\omega, \mathbf{k}_T, \sigma) \\ &\times e^{-j(\omega t - \mathbf{k}_T \cdot \boldsymbol{\rho} - \sqrt{\omega^2/c^2 - |\mathbf{k}_T|^2} z)} \mathbf{e}_{\omega, \mathbf{k}_T, \sigma} \end{aligned} \quad (12)$$

where $\boldsymbol{\rho} = (x, y)$ and $\mathbf{k}_T = (k_x, k_y)$ are the transverse components of \mathbf{r} and \mathbf{k} , respectively, and the commutator from (10) is replaced by

$$\begin{aligned} [\hat{A}(\omega, \mathbf{k}_T, \sigma), \hat{A}^\dagger(\omega', \mathbf{k}'_T, \sigma')] &= c\sqrt{1 - \left(\frac{c|\mathbf{k}_T|}{\omega}\right)^2} \\ &\times (2\pi)^3 \delta(\omega - \omega') \delta(\mathbf{k}_T - \mathbf{k}'_T) \delta_{\sigma\sigma'}. \end{aligned} \quad (13)$$

Now, we define the $+z$ -propagating positive-frequency field operators in the $z = 0$ and $z = L$ planes by

$$\hat{\mathbf{E}}_0^{(+)}(\boldsymbol{\rho}, t) = \hat{\mathbf{E}}_{(+)}^{(+)}(\mathbf{r}, t)|_{\mathbf{r}=(\boldsymbol{\rho}, z=0)} \quad (14)$$

$$\hat{\mathbf{E}}_L^{(+)}(\boldsymbol{\rho}', t) = \hat{\mathbf{E}}_{(+)}^{(+)}(\mathbf{r}, t)|_{\mathbf{r}=(\boldsymbol{\rho}', z=L)} \quad (15)$$

which can be combined with (12) to get

$$\hat{\mathbf{E}}_L^{(+)}(\boldsymbol{\rho}', t') = \int d^2\boldsymbol{\rho} \int dt \hat{\mathbf{E}}_0^{(+)}(\boldsymbol{\rho}, t) h_L(\boldsymbol{\rho}' - \boldsymbol{\rho}, t' - t) \quad (16)$$

with

$$\begin{aligned} h_L(\boldsymbol{\rho}, t) &\equiv \int_0^\infty \frac{d\omega}{2\pi} \int_{|\mathbf{k}_T| < \omega/c} \frac{d^2\mathbf{k}_T}{(2\pi)^2} \\ &\times e^{-j(\omega t - \mathbf{k}_T \cdot \boldsymbol{\rho} - \sqrt{\omega^2/c^2 - |\mathbf{k}_T|^2} L)} \end{aligned} \quad (17)$$

being the Green's function (spatiotemporal impulse response) for diffraction over an L -meter-long free-space path.

Equations (16) and (17) realize the boundary-value approach to field operator propagation. Thus, in particular, they can be used to deduce the state that will be received over the entrance pupil \mathcal{A}_L in Fig. 1, given the state of the field that is emitted through the exit pupil \mathcal{A}_0 in that figure. However, before showing how this can be accomplished, it is worthwhile to simplify these equations by imposing realistic conditions for free-space optical communications. Specifically, we shall assume that the transmitter only excites plane-wave modes within a narrow frequency band around a center frequency ω_0 , and that the exit and entrance pupils in Fig. 1 are such that the receiver only measures plane-wave modes, within this excited frequency band, for which $|\mathbf{k}_T| \ll \omega_0/c$. Furthermore, we shall neglect the possibility of using polarization modulation by assuming that the transmitter only excites a single linear polarization component of the field in its exit pupil. Under these single-polarization, quasi-monochromatic, and paraxial conditions, we can take the relevant positive-frequency scalar field operator in the $z = 0$ plane to be

$$\hat{E}_0(\boldsymbol{\rho}, t) = \int \frac{d\omega}{2\pi} \int \frac{d^2\mathbf{k}_T}{(2\pi)^2} \hat{A}_0(\omega, \mathbf{k}_T) e^{-j(\omega t - \mathbf{k}_T \cdot \boldsymbol{\rho})}. \quad (18)$$

Here, we have suppressed factors that are approximately constant for quasi-monochromatic paraxial modes, so that \hat{E}_0 has units $\sqrt{\text{photons/m}^2\text{s}}$ and

$$[\hat{A}_0(\omega, \mathbf{k}_T), \hat{A}_0^\dagger(\omega', \mathbf{k}'_T)] = (2\pi)^3 \delta(\omega - \omega') \delta(\mathbf{k}_T - \mathbf{k}'_T) \quad (19)$$

is the relevant Fourier-domain commutator. Note that we have exploited the quasi-monochromatic paraxial condition to extend the regions of integration to run from $-\infty$ to ∞ for ω , k_x , and k_y , i.e., we have now included negative frequencies and evanescent waves that are clearly inappropriate for the positive-frequency $+z$ -propagating field operator. However, these frequencies and wave vectors will neither be excited by the transmitter nor measured by the receiver; therefore, their inclusion—though it may be egregious in a general setting—causes no harm in our quasi-monochromatic, paraxial propagation scenario.

To complete our simplification of free-space quantum diffraction, we impose the quasi-monochromatic and paraxial conditions on the Green's function in (17), from which it follows that

$$\hat{E}_L(\boldsymbol{\rho}', t) = \int \frac{d\omega}{2\pi} \int \frac{d^2 \mathbf{k}_T}{(2\pi)^2} \hat{A}_L(\omega, \mathbf{k}_T) e^{-j(\omega t - \mathbf{k}_T \cdot \boldsymbol{\rho}')} \quad (20)$$

where

$$[\hat{A}_L(\omega, \mathbf{k}_T), \hat{A}_L^\dagger(\omega', \mathbf{k}'_T)] = (2\pi)^3 \delta(\omega - \omega') \delta(\mathbf{k}_T - \mathbf{k}'_T) \quad (21)$$

because the Fourier-domain field operator \hat{A}_L is given by the quasi-monochromatic paraxial diffraction formula

$$\hat{A}_L(\omega, \mathbf{k}_T) = \hat{A}_0(\omega, \mathbf{k}_T) e^{j(\omega L/c - c|\mathbf{k}_T|^2 L/2\omega_0)}. \quad (22)$$

Combining these results, we obtain the quantum form of the Huygens–Fresnel diffraction integral for quasi-monochromatic light:

$$\hat{E}_L(\boldsymbol{\rho}', t) = \int d^2 \boldsymbol{\rho} \hat{E}_0\left(\boldsymbol{\rho}, t - \frac{L}{c}\right) \frac{e^{j(k_0 L + k_0 |\boldsymbol{\rho}' - \boldsymbol{\rho}|^2/2L)}}{j\lambda_0 L} \quad (23)$$

where $k_0 \equiv \omega_0/c$ is the wavenumber at the center frequency and $\lambda_0 \equiv 2\pi c/\omega_0$ is the wavelength at that center frequency. The positive-frequency photon-units field operators at the input and output planes share the common δ -function commutator

$$[\hat{E}_z(\boldsymbol{\rho}_1, t_1), \hat{E}_z^\dagger(\boldsymbol{\rho}_2, t_2)] = \delta(\boldsymbol{\rho}_1 - \boldsymbol{\rho}_2) \delta(t_1 - t_2), \quad \text{for } z = 0, L \quad (24)$$

ensuring that the same free-field Heisenberg uncertainty principle is satisfied in both locations.

We now have a free-space propagation formula for quantum field operators that mimics the classical version. Indeed, the classical result [34] is recovered by averaging on both sides of (24), thus yielding

$$E_L(\boldsymbol{\rho}', t) = \int d^2 \boldsymbol{\rho} E_0\left(\boldsymbol{\rho}, t - \frac{L}{c}\right) \frac{e^{j(\omega_0 L + k_0 |\boldsymbol{\rho}' - \boldsymbol{\rho}|^2/2L)}}{j\lambda_0 L} \quad (25)$$

where $E_z(\boldsymbol{\rho}, t) \equiv \langle \hat{E}_z(\boldsymbol{\rho}, t) \rangle$, for $z = 0, L$, are the mean fields at the input and output planes, and $\hbar\omega_0 |E_z(\boldsymbol{\rho}, t)|^2$ is the short-time average power density crossing the z -plane in the $+z$ -direction

at time t . It follows that the same modal decomposition that applies to \mathcal{A}_0 -to- \mathcal{A}_L coupling in the classical case can be applied to the quantum situation. As we shall see, the quantum modal decomposition makes obtaining the state of \hat{E}_L , given the state of \hat{E}_0 , a relatively simple task.

C. Normal-Mode Decomposition for Free-Space Diffraction

To introduce the normal-mode decomposition, it is convenient to start from the classical case [21]. Suppose that the transmitter emits a classical field in the $z = 0$ plane that can only be nonzero in the \mathcal{A}_0 pupil, and suppose that the receiver can only measure the field in the $z = L$ plane that enters through the \mathcal{A}_L pupil. The classical free-space diffraction formula with these restrictions is then

$$E_L(\boldsymbol{\rho}', t) = \int_{\mathcal{A}_0} d^2 \boldsymbol{\rho} E_0\left(\boldsymbol{\rho}, t - \frac{L}{c}\right) h_L(\boldsymbol{\rho}' - \boldsymbol{\rho}), \quad \text{for } \boldsymbol{\rho}' \in \mathcal{A}_L \quad (26)$$

where

$$h_L(\boldsymbol{\rho}) \equiv \frac{e^{j(k_0 L + k_0 |\boldsymbol{\rho}|^2/2L)}}{j\lambda_0 L}. \quad (27)$$

The normal-mode decomposition of (26) follows from the singular value decomposition of $h_L(\boldsymbol{\rho} - \boldsymbol{\rho}')$ for $\boldsymbol{\rho} \in \mathcal{A}_0$ and $\boldsymbol{\rho}' \in \mathcal{A}_L$. It is composed of complete orthonormal (CON) sets of input and output eigenfunctions $\{\Phi_n(\boldsymbol{\rho}) : 1 \leq n < \infty, \boldsymbol{\rho} \in \mathcal{A}_0\}$ and $\{\phi_n(\boldsymbol{\rho}') : 1 \leq n < \infty, \boldsymbol{\rho}' \in \mathcal{A}_L\}$, respectively, and associated nonnegative eigenvalues $\{\eta_n : 1 \leq n < \infty\}$, such that

$$h_L(\boldsymbol{\rho}' - \boldsymbol{\rho}) = \sum_n \sqrt{\eta_n} \phi_n(\boldsymbol{\rho}') \Phi_n^*(\boldsymbol{\rho}). \quad (28)$$

Expanding $E_0(\boldsymbol{\rho}, t)$ in terms of the input eigenfunctions

$$E_0(\boldsymbol{\rho}, t) = \sum_n a_n(t) \Phi_n(\boldsymbol{\rho}), \quad \text{for } \boldsymbol{\rho} \in \mathcal{A}_0 \quad (29)$$

leads to

$$E_L(\boldsymbol{\rho}', t) = \sum_n \sqrt{\eta_n} a_n\left(t - \frac{L}{c}\right) \phi_n(\boldsymbol{\rho}'), \quad \text{for } \boldsymbol{\rho}' \in \mathcal{A}_L \quad (30)$$

as the output-eigenfunction expansion for $E_L(\boldsymbol{\rho}', t)$, where

$$a_n(t) \equiv \int_{\mathcal{A}_0} d^2 \boldsymbol{\rho} E_0(\boldsymbol{\rho}, t) \Phi_n^*(\boldsymbol{\rho}). \quad (31)$$

When the transmitter's output is time-limited to a finite interval $0 \leq t \leq T$, it can be convenient to expand $\{a_n(t)\}$ in a generalized Fourier series

$$a_n(t) = \sum_m a_{nm} \theta_m(t), \quad \text{for } 0 \leq t \leq T \quad (32)$$

where $\{\theta_m(t)\}$ is a CON function set on this domain and

$$a_{nm} \equiv \int_0^T dt a_n(t) \theta_m^*(t). \quad (33)$$

We now have that transmitting

$$E_0(\boldsymbol{\rho}, t) = \sum_{n,m} a_{nm} \Phi_n(\boldsymbol{\rho}) \theta_m(t), \quad \text{for } \boldsymbol{\rho} \in \mathcal{A}_0, 0 \leq t \leq T \quad (34)$$

produces the received field

$$E_L(\boldsymbol{\rho}', t) = \sum_{n,m} \sqrt{\eta_n} a_{nm} \phi_n(\boldsymbol{\rho}) \theta_m \left(t - \frac{L}{c} \right),$$

$$\text{for } \boldsymbol{\rho}' \in \mathcal{A}_L, \quad 0 \leq t - \frac{L}{c} \leq T. \quad (35)$$

These equations decompose the classical free-space channel for communication between the \mathcal{A}_0 and \mathcal{A}_L pupils over a T -second-long time interval into a set of orthogonal (parallel-channel) spatiotemporal modes such that excitation of the transmitter mode $\Phi_n(\boldsymbol{\rho})\theta_m(t)$ with complex amplitude a_{nm} gives rise to a $\sqrt{\eta_n} a_{nm}$ excitation of the receiver mode $\phi_n(\boldsymbol{\rho}')\theta_m(t - L/c)$. Hence, because $\hbar\omega_0|a_{nm}|^2$ is the energy contained in an a_{nm} excitation of the nm th spatiotemporal input mode, and because the quasi-monochromatic Huygens–Fresnel principle is not dispersive in time, we see that η_n is the fraction of the transmitted power from the n th spatial mode that is collected by the receiver. That free-space diffraction is a passive process tells us that $\eta_n \leq 1$. Without loss of generality, we can arrange the spatial modes, so that the eigenvalues occur in nonincreasing order, i.e., $1 \geq \eta_1 \geq \eta_2 \geq \eta_3 \geq \dots \geq 0$.

From a classical communication theory standpoint, it is the power-transfer characteristics of the eigenvalues that determine channel capacity [35]. Although results are available for the eigenvalue behavior when the transmitter and receiver employ coaxial circular pupils, it is enough for us to note the following key points about this case [21], [36]. The sum of the eigenvalues equals the Fresnel number product of the two pupils:

$$\mathcal{D}_f \equiv \sum_n \eta_n = \int_{\mathcal{A}_0} d^2\boldsymbol{\rho} \int_{\mathcal{A}_L} d^2\boldsymbol{\rho}' |h_L(\boldsymbol{\rho}' - \boldsymbol{\rho})|^2 \quad (36)$$

$$= \frac{A_0 A_L}{(\lambda_0 L)^2} \quad (37)$$

where A_z is the area of the \mathcal{A}_z pupil. When $\mathcal{D}_f \ll 1$, we are in the far-field power-transfer regime, wherein only one mode couples appreciable power from \mathcal{A}_0 to \mathcal{A}_L because $\eta_1 \approx \mathcal{D}_f$. When $\mathcal{D}_f \gg 1$, we are in the near-field power-transfer regime, wherein

$$\eta_n \approx \begin{cases} 1, & \text{for } 1 \leq n \leq \mathcal{D}_f \\ 0, & \text{otherwise.} \end{cases} \quad (38)$$

Although it might be tempting to replace the phasors $\{a_{nm}\}$ with annihilation operators $\{\hat{a}_{nm}\}$ and assert that

$$\hat{E}_0(\boldsymbol{\rho}, t) = \sum_{n,m} \hat{a}_{nm} \Phi_n(\boldsymbol{\rho}) \theta_m(t), \quad \text{for } \boldsymbol{\rho} \in \mathcal{A}_0, \quad 0 \leq t \leq T \quad (39)$$

and

$$\hat{E}_L(\boldsymbol{\rho}', t) = \sum_{n,m} \sqrt{\eta_n} \hat{a}_{nm} \phi_n(\boldsymbol{\rho}') \theta_m \left(t - \frac{L}{c} \right),$$

$$\text{for } \boldsymbol{\rho}' \in \mathcal{A}_L, \quad 0 \leq t - \frac{L}{c} \leq T \quad (40)$$

provide the quantum versions of (34) and (35), such is *not* the case. There is no problem with (39), because it preserves the commutator structure from (24) within its domain

of applicability. In contrast, (40) does *not* lead to the proper free-field commutator for $\boldsymbol{\rho}' \in \mathcal{A}_L$ and $0 \leq t - L/c \leq T$. What is needed, in lieu of (40), is

$$\hat{E}_L(\boldsymbol{\rho}', t) = \sum_{n,m} (\sqrt{\eta_n} \hat{a}_{nm} + \sqrt{1 - \eta_n} \hat{e}_{nm}) \phi_n(\boldsymbol{\rho}') \times \theta_m \left(t - \frac{L}{c} \right), \quad \text{for } \boldsymbol{\rho}' \in \mathcal{A}_L, \quad 0 \leq t - \frac{L}{c} \leq T \quad (41)$$

where $\{\hat{e}_{nm}\}$ is a set of photon annihilation operators associated with unexcited $+z$ -propagating spatiotemporal modes arising from *outside* the \mathcal{A}_0 pupil that couple power into the \mathcal{A}_L pupil.¹ In this quantum normal-mode decomposition, we see that the state of the transmitter field can be specified as a joint density operator for the input modes associated with $\{\hat{a}_{nm}\}$. The state of the field entering the receiver can then be obtained by finding the joint density operator for the output modes associated with $\{\hat{b}_{nm} \equiv \sqrt{\eta_n} \hat{a}_{nm} + \sqrt{1 - \eta_n} \hat{e}_{nm}\}$. These annihilation operator input–output relations are beam splitter transformations, for which characteristic functions provide a conceptually simple and completely general solution for the state-transformation problem as the following example will show.

Consider a far-field communication problem in which the transmitter only excites the $\Phi_1(\boldsymbol{\rho})\theta_1(t)$ mode, placing it in a state given by the density operator $\hat{\rho}_{\text{in}}$ and leading to the received mode $\phi_1(\boldsymbol{\rho}')\theta_1(t - L/c)$ being in the state given by the density operator $\hat{\rho}_{\text{out}}$. Using the fact that the density operator $\hat{\rho}$ for a bosonic mode with annihilation operator \hat{a} is completely determined by its antinormally ordered characteristic function

$$\chi_A^\rho(\zeta^*, \zeta) \equiv \text{tr}(\hat{\rho} e^{-\zeta^* \hat{a}} e^{\zeta \hat{a}^\dagger}) \quad (42)$$

plus $\hat{b}_{11} = \sqrt{\eta_1} \hat{a}_{11} + \sqrt{1 - \eta_1} \hat{e}_{11}$ with the \hat{e}_{11} mode in its vacuum state, we find that [20]

$$\chi_A^{\rho_{\text{out}}}(\zeta^*, \zeta) = \chi_A^{\rho_{\text{in}}}(\sqrt{\eta_1} \zeta^*, \sqrt{\eta_1} \zeta) e^{-(1 - \eta_1)|\zeta|^2}. \quad (43)$$

In Section III, we shall see that even simpler state-transformation relations apply when the transmitted field is in a Gaussian state.

III. GAUSSIAN STATES

Gaussian states are important in both classical and quantum information transmission using lightwaves. Their single- and two-mode descriptions are well known in quantum optics, but their behavior for spatiotemporal field operators is not as well appreciated. In this section, therefore, we will briefly review the single- and two-mode cases, and then dwell upon the full field-operator scenarios.

A. Single-Mode and Two-Mode Gaussian States

The Gaussian states of a single-mode quantum field with annihilation operator \hat{a} and frequency ω_0 are the quantum analogs of $ae^{-j\omega_0 t}$, where a is a complex-valued Gaussian random variable. Thus, they can be defined as having characteristic functions

¹In Section V, we shall allow these environmental modes to be in thermal states when we consider the classical information capacities of bosonic channels.

that are Gaussian forms. The coherent states of the \hat{a} mode are the eigenkets of that annihilation operator [23]

$$\hat{a}|\alpha\rangle = \alpha|\alpha\rangle \quad (44)$$

for α being a complex number. The coherent states are Gaussian because their antinormally ordered characteristic function is the Gaussian form

$$\chi_A^{|\alpha\rangle\langle\alpha|}(\zeta^*, \zeta) = \langle\alpha|e^{-\zeta^*\hat{a}}e^{\zeta\hat{a}^\dagger}|\alpha\rangle = e^{-\zeta^*\alpha + \zeta\alpha^* - |\zeta|^2}. \quad (45)$$

Physically, the coherent states give the classical limit of noiseless simple harmonic motion for $\hat{a}(t) = \hat{a}e^{-j\omega_0 t}$ [23]. They are the states produced by classical current distributions and by ideal lasers, and they satisfy

$$\frac{\langle\alpha|\hat{a}(t)|\alpha\rangle}{\alpha} = e^{-j\omega_0 t} \quad (46)$$

with

$$\lim_{|\alpha| \rightarrow \infty} \left(\frac{\langle\alpha|\Delta\hat{a}_1^2|\alpha\rangle}{|\alpha|^2} \right) = \lim_{|\alpha| \rightarrow \infty} \left(\frac{\langle\alpha|\Delta\hat{a}_2^2|\alpha\rangle}{|\alpha|^2} \right) = 0 \quad (47)$$

for $\Delta\hat{a}_1 \equiv \text{Re}(\hat{a} - \langle\hat{a}\rangle)$ and $\Delta\hat{a}_2 \equiv \text{Im}(\hat{a} - \langle\hat{a}\rangle)$ being the fluctuations in the real and imaginary quadratures of \hat{a} .

A zero-mean, isotropic Gaussian mixture of coherent states with average photon number N has the density operator

$$\hat{\rho} = \int d^2\alpha \frac{e^{-|\alpha|^2/N}}{\pi N} |\alpha\rangle\langle\alpha| \quad (48)$$

making its antinormally ordered characteristic function equal to

$$\chi_A^\rho(\zeta^*, \zeta) = e^{-(1+N)|\zeta|^2}. \quad (49)$$

Therefore, it too is a Gaussian state. If the \hat{a} mode is in thermal equilibrium at temperature T_0 , then its density operator will be given by (48) with $N = 1/(e^{\hbar\omega_0/k_B T_0} - 1)$, where k_B is Boltzmann's constant. Thus, (48) is frequently referred to as a thermal state, even when N is not given by the Planck relation.

The squeezed states $|\beta; \mu, \nu\rangle$ are the eigenkets of the annihilation operator \hat{b} obtained from the Bogoliubov transformation [37]

$$\hat{b} \equiv \mu\hat{a} + \nu\hat{a}^\dagger, \quad \text{with } |\mu|^2 - |\nu|^2 = 1 \quad (50)$$

i.e.,

$$\hat{b}|\beta; \mu, \nu\rangle = \beta|\beta; \mu, \nu\rangle \quad (51)$$

for β being a complex number. They are Gaussian states because their antinormally ordered characteristic function is

$$\begin{aligned} \chi_A^{|\beta; \mu, \nu\rangle\langle\beta; \mu, \nu|}(\zeta^*, \zeta) &= e^{-\zeta^*(\mu^*\beta - \nu\beta^*) + \zeta(\mu\beta^* - \nu^*\beta)} \\ &\times e^{-(1+|\nu|^2)|\zeta|^2 - \text{Re}(\mu^*\nu\zeta^*\zeta^*)}. \end{aligned} \quad (52)$$

Squeezed states can be produced by parametric amplification [38]. They offer an SNR advantage over coherent states of the same average photon number in homodyne detection [39]. As a result, they hold promise for improving the performance of precision measurement systems [24], [25], [40].

For two modes of the quantized field with annihilation operators \hat{a}_S and \hat{a}_I —for signal (S) and idler (I), as in optical parametric interactions—the two-mode squeezed-vacuum state

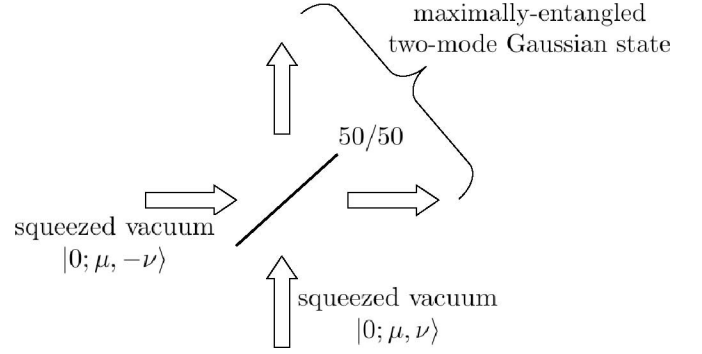


Fig. 2. Scheme for generating a maximally entangled two-mode Gaussian state from two squeezed-vacuum states.

$|\psi\rangle_{SI}$ is the Gaussian state whose antinormally ordered characteristic function is

$$\begin{aligned} \chi_A^{|\psi\rangle_{SI}\langle\psi|}(\zeta_S^*, \zeta_S; \zeta_I^*, \zeta_I) &\equiv {}_{SI}\langle\psi|e^{-\zeta_S^*\hat{a}_S - \zeta_I^*\hat{a}_I}e^{\zeta_S\hat{a}_S^\dagger + \zeta_I\hat{a}_I^\dagger}|\psi\rangle_{SI} \\ &= e^{-(1+|\nu|^2)(|\zeta_S|^2 + |\zeta_I|^2) + 2\text{Re}(\mu^*\nu\zeta_S^*\zeta_I^*)}. \end{aligned} \quad (53)$$

Physically, this is the maximally entangled state formed by combining a pair of single-mode squeezed-vacuum states—squeezed states with $\beta = 0$ —on a 50–50 beam splitter, as shown in Fig. 2 and used in quadrature-based teleportation [16].

B. Gaussian States of Spatiotemporal Field Operators

Although the preceding section amply illustrates the importance of single-mode and two-mode Gaussian states, it fails to convey the full richness of such states. This richness appears when we examine Gaussian states of spatiotemporal field operators. Here, we will illustrate that behavior in the specific context of the quantum diffraction scenario from Section II-B. The scalar, $+z$ -going, photon-units, positive-frequency, field operator $\hat{E}_0(\rho, t)$ is in a Gaussian state if its antinormally ordered characteristic functional takes the Gaussian form

$$\chi_A^\rho[\zeta^*(\rho, t), \zeta(\rho, t)] \equiv \text{tr}(e^{-\zeta^*\hat{a}}e^{\zeta\hat{a}^\dagger}) \quad (54)$$

$$= e^{-\xi^*(\hat{a}) + \xi(\hat{a})^* - (1 + \langle\Delta\hat{a}^\dagger\Delta\hat{a}\rangle)|\xi|^2 + \text{Re}(\langle\Delta\hat{a}^2\rangle\xi^{*2})} \quad (55)$$

where $\zeta(\rho, t) = \xi\psi(\rho, t)$, with ξ being a complex number

$$\hat{a} \equiv \int d^2\rho \int dt \psi^*(\rho, t)\hat{E}_0(\rho, t) \quad (56)$$

$\Delta\hat{a} \equiv \hat{a} - \langle\hat{a}\rangle$, and $\psi(\rho, t)$ is a deterministic function satisfying

$$\int d^2\rho \int dt |\psi(\rho, t)|^2 = 1. \quad (57)$$

From Section II-C, we see that \hat{a} is the annihilation operator associated with $\psi(\rho, t)$ mode of $\hat{E}_0(\rho, t)$. From Section III-A, we see that every such mode of a Gaussian-state field operator $\hat{E}_0(\rho, t)$ is in a single-mode Gaussian state. Indeed, with scarcely more work, it can be shown that *any* collection of modes from a Gaussian-state field operator is in a jointly

Gaussian state.² More importantly, we have

$$\langle \hat{a} \rangle = \int d^2 \rho \int dt \psi^*(\rho, t) \langle \hat{E}_0(\rho, t) \rangle \quad (58)$$

$$\begin{aligned} \langle \Delta \hat{a}^\dagger \Delta \hat{a} \rangle &= \int d^2 \rho_1 \int dt_1 \int d^2 \rho_2 \int dt_2 \psi(\rho_1, t_1) \\ &\quad \times \psi^*(\rho_2, t_2) \langle \Delta \hat{E}_0^\dagger(\rho_1, t_1) \Delta \hat{E}_0(\rho_2, t_2) \rangle \end{aligned} \quad (59)$$

$$\begin{aligned} \langle \Delta \hat{a}^2 \rangle &= \int d^2 \rho_1 \int dt_1 \int d^2 \rho_2 \int dt_2 \psi^*(\rho_1, t_1) \\ &\quad \times \psi^*(\rho_2, t_2) \langle \Delta \hat{E}_0(\rho_1, t_1) \Delta \hat{E}_0(\rho_2, t_2) \rangle \end{aligned} \quad (60)$$

where $\Delta \hat{E}_0(\rho, t) \equiv \hat{E}_0(\rho, t) - \langle \hat{E}_0(\rho, t) \rangle$. Thus, the general Gaussian state of a field operator $\hat{E}_0(\rho, t)$ is completely characterized [41] by knowledge of its mean field $\langle \hat{E}_0(\rho, t) \rangle$, its phase-insensitive (normally ordered) covariance function

$$K_{E_0 E_0}^{(n)}(\rho_1, t_1; \rho_2, t_2) \equiv \langle \Delta \hat{E}_0^\dagger(\rho_1, t_1) \Delta \hat{E}_0(\rho_2, t_2) \rangle \quad (61)$$

and its phase-sensitive covariance function

$$K_{E_0 E_0}^{(p)}(\rho_1, t_1; \rho_2, t_2) \equiv \langle \Delta \hat{E}_0(\rho_1, t_1) \Delta \hat{E}_0(\rho_2, t_2) \rangle. \quad (62)$$

That first and second moments suffice to specify a Gaussian state is the quantum analog of the corresponding property for classical Gaussian random processes. Other significant properties of Gaussian random processes also carry over to Gaussian states. Of special note, for the quantum theory of optical communications, is the fact that Gaussian states are closed under linear transformations. Consequently, in the Fig. 1 propagation geometry, if $\hat{E}_0(\rho, t)$ for $\rho \in \mathcal{A}_0$ and $0 \leq t \leq T$ is in a Gaussian state, then the linearity of the quantum Huygens–Fresnel principle implies that $\hat{E}_L(\rho', t')$ for $\rho' \in \mathcal{A}_L$ and $0 \leq t' - L/c \leq T$ will also be in a Gaussian state. The output state's specification is then completed by using (25) to obtain $\langle \hat{E}_L(\rho', t') \rangle$ from $\langle \hat{E}_0(\rho, t) \rangle$, and straightforward quantum-coherence-theory calculations to evaluate $K_{E_L E_L}^{(n)}(\rho'_1, t'_1; \rho'_2, t'_2)$ and $K_{E_L E_L}^{(p)}(\rho'_1, t'_1; \rho'_2, t'_2)$ from the corresponding $\hat{E}_0(\rho, t)$ covariances [42].

For our treatment of HOM interferometry and the CHSH inequality, we will need the joint Gaussian state of two field operators $\hat{E}_S(\rho, t)$ and $\hat{E}_I(\rho, t)$, which represent the signal and idler fields from a parametric downconverter. Such a joint state has a Gaussian antinormally ordered characteristic functional that only involves the mean fields, the phase-insensitive and phase-sensitive autocovariance functions of the two fields $K_{E_K E_K}^{(n)}$ and $K_{E_K E_K}^{(p)}$, for $K = S, I$, and their cross-covariance functions

$$K_{E_S E_I}^{(n)}(\rho_1, t_1; \rho_2, t_2) = \langle \Delta \hat{E}_S^\dagger(\rho_1, t_1) \Delta \hat{E}_I(\rho_2, t_2) \rangle \quad (63)$$

$$K_{E_S E_I}^{(p)}(\rho_1, t_1; \rho_2, t_2) = \langle \Delta \hat{E}_S(\rho_1, t_1) \Delta \hat{E}_I(\rho_2, t_2) \rangle. \quad (64)$$

²This is just the quantum version of the following well-known result from classical random process theory. For $x(t)$ being a real-valued Gaussian random process, and $\{\phi_n(t) : 1 \leq n \leq N\}$ being a set of real-valued orthonormal mode functions, the random variables $\{x_n \equiv \int dt x(t) \phi_n(t) : 1 \leq n \leq N\}$ are jointly Gaussian.

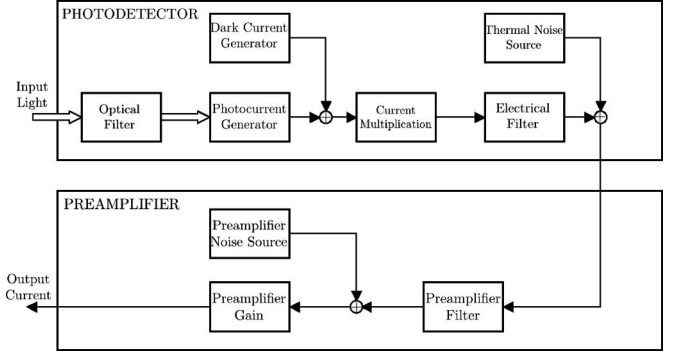


Fig. 3. Phenomenological block diagram of a photodetection system. Wide arrows denote optical signals and thin arrows denote electrical currents.

Because classical Gaussian random processes are determined by their first and second moments, all higher order moments can be expressed in terms of these low-order moments via the Gaussian moment factoring theorem [43]. The same is true for the Gaussian states of quantum field operators, and this property will be of use, in Section IV, when we examine photon-coincidence counting in HOM and CHSH experiments. As a preview of what will be seen there, we note that if two field operators $\hat{E}_A(\rho, t)$ and $\hat{E}_B(\rho', t')$ are in a zero-mean jointly Gaussian state, then

$$\begin{aligned} \langle \hat{E}_A^\dagger(\rho, t) \hat{E}_A(\rho, t) \hat{E}_B^\dagger(\rho', t') \hat{E}_B(\rho', t') \rangle &= K_{E_A E_A}^{(n)}(\rho, t; \rho, t) \\ &\quad \times K_{E_B E_B}^{(n)}(\rho', t'; \rho', t') + |K_{E_A E_B}^{(n)}(\rho, t; \rho', t')|^2 \\ &\quad + |K_{E_A E_B}^{(p)}(\rho, t; \rho', t')|^2. \end{aligned} \quad (65)$$

IV. SEMICLASSICAL VERSUS QUANTUM PHOTODETECTION

Fig. 3 shows a block diagram for a photodetection system whose two large blocks represent the photodetector and its post-detection preamplifier. Contained within these large blocks are smaller blocks that account for the principal photodetection phenomena, even though they may not be explicitly identifiable as separate elements within a real photodetector. Incoming light—whether we model it in classical or quantum terms—illuminates an optical filter that models the wavelength dependence of the photodetector's sensitivity. The light emerging from this filter then strikes the core of the photodetector, i.e., the block that converts light into a light-induced current, which we call the photocurrent. Photodetectors have some current flow in the absence of illumination, and this dark current adds to the photocurrent within the detector. High-sensitivity photodetectors—such as avalanche photodiodes and photomultiplier tubes—have internal mechanisms that amplify (multiply) the initial photocurrent (and the dark current), which is shown in Fig. 3 as the current multiplication block. This current multiplication, in general, has some randomness associated with it, imposing an excess noise on top of any noise already inherent in the photocurrent and dark current. The electrical filter that is next encountered models the electrical bandwidth of the photodetector's output circuit, and the thermal noise generator models the noise associated

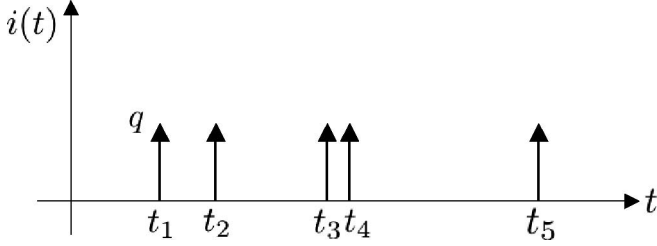


Fig. 4. Train of charge- q current impulses produced by photodetection under idealized conditions.

with the dissipative elements in the detector. Because the output current from a photodetector may not be strong enough to regard all subsequent processing as noiseless, we have included the preamplifier block in Fig. 3. Its filter, noise generator, and gain blocks model the bandwidth characteristics, noise figure, and gain of a real preamplifier. Ordinarily, the output from such a preamplifier is strong enough that any further signal processing can be regarded as noise-free.

Having surveyed the phenomenology of photodetection, we shall now dispense with almost all of it to focus on the *fundamental* noise source, i.e., that associated with converting the illuminating field into a photocurrent. To do so, we shall assume that the photodetector has the following properties: its optical sensitivity covers all frequencies with constant efficiency $\eta \leq 1$, it has no dark current, it has no internal current multiplication, and its electrical bandwidth is infinite. The preamplifier will be assumed to have infinite bandwidth and no noise; therefore, it will not be considered any further as it does not affect photodetection performance. Under these conditions, the photocurrent $i(t)$ is a train of area- q impulses, where q is the electron charge, as shown in Fig. 4. The semiclassical and quantum theories of photodetection, which will be the subject of this section, provide alternative statistical descriptions for the Fig. 4 photocurrent impulse train.

A. Semiclassical Theory

In the semiclassical theory of photodetection, the light impinging on the detector's photosensitive region is taken to be a classical electromagnetic field. To ease comparison with the quantum theory that will be presented in Section IV-B, and in keeping with the propagation theory from Section III, we shall take this classical electromagnetic field to be a $+z$ propagating, scalar, quasi-monochromatic, paraxial wave specified by the $\sqrt{\text{photons/m}^2\text{s}}$ -units, positive-frequency field $E(\boldsymbol{\rho}, t)$, where $\boldsymbol{\rho}$ is the transverse vector in the z -plane containing the detector's photosensitive region \mathcal{A}_d . In general, this field will be a random process, which will contribute excess noise to the photocurrent $i(t)$. Even if the field is nonrandom, there will still be noise in $i(t)$: the shot noise associated with the discreteness of the electron charge and the random times at which current impulses carrying this charge are produced in response to illumination.

1) *Direct Detection*: In the absence of extraneous background light, the only field illuminating the photodetector in a direct-detection system is the signal light of interest. The

photocurrent is a train of impulses

$$i(t) = \sum_n q\delta(t - t_n) \quad (66)$$

and hence, its statistics are those of the point process $\{t_n\}$. If we limit our attention to the time interval $0 \leq t \leq T$, and condition the statistics on knowledge of the short-time average illumination power

$$P(t) \equiv \hbar\omega_0 \int_{\mathcal{A}_d} d^2\boldsymbol{\rho} |E(\boldsymbol{\rho}, t)|^2 \quad (67)$$

then $\{t_n : 0 \leq t_n \leq T\}$ is an inhomogeneous Poisson point process with rate function [6], [44]

$$\gamma(t) = \frac{\eta P(t)}{\hbar\omega_0} = \eta \int_{\mathcal{A}_d} d^2\boldsymbol{\rho} |E(\boldsymbol{\rho}, t)|^2. \quad (68)$$

Thus, given knowledge of the power waveform, the photocount

$$N(t) \equiv \frac{1}{q} \int_0^t d\tau i(\tau) \quad (69)$$

i.e., the number of current impulses that have occurred between the initial time and time t , is an inhomogeneous Poisson counting process with rate $\gamma(t)$. Hence, we have

$$\begin{aligned} \Pr(N(t) = n \mid \{P(\tau) : 0 \leq \tau \leq t\}) \\ = \frac{\left(\int_0^t d\tau \gamma(\tau)\right)^n e^{-\int_0^t d\tau \gamma(\tau)}}{n!}, \quad \text{for } n = 0, 1, 2, \dots \end{aligned} \quad (70)$$

for the conditional statistics of this process. When the illumination is a random process, we use Mandel's rule [45] to obtain the probability distribution for the unconditional photocount

$$\begin{aligned} \Pr(N(t) = n) = \left\langle \frac{\left(\int_0^t d\tau \gamma(\tau)\right)^n e^{-\int_0^t d\tau \gamma(\tau)}}{n!} \right\rangle, \\ \text{for } n = 0, 1, 2, \dots \end{aligned} \quad (71)$$

where $\langle \cdot \rangle$ denotes averaging over the statistics of the rate function $\gamma(t)$. As an example, suppose that

$$E(\boldsymbol{\rho}, t) = a\psi(\boldsymbol{\rho}, t), \quad \text{for } \boldsymbol{\rho} \in \mathcal{A}_d, \quad 0 \leq t \leq T \quad (72)$$

where $\psi(\boldsymbol{\rho}, t)$ is a deterministic mode function obeying the normalization condition

$$\int_{\mathcal{A}_d} d^2\boldsymbol{\rho} \int_0^T dt |\psi(\boldsymbol{\rho}, t)|^2 = 1 \quad (73)$$

and a is a zero-mean, isotropic, complex-valued Gaussian random variable with $\langle |a|^2 \rangle = N$. In this case, Mandel's rule gives a Bose-Einstein distribution for the unconditional photocount at time $t = T$

$$\Pr(N(T) = n) = \frac{(\eta N)^n}{(\eta N + 1)^{n+1}}, \quad \text{for } n = 0, 1, 2, \dots \quad (74)$$

whose mean and variance are

$$\langle N(T) \rangle = \eta N \quad (75)$$

and

$$\langle [\Delta N(T)]^2 \rangle = \eta N + (\eta N)^2 \quad (76)$$

where $\Delta N(T) \equiv N(T) - \langle N(T) \rangle$.

Equations (75) and (76) exemplify the division between shot noise and excess noise, and the fundamental signal-to-noise limit imposed by the former on direct-detection systems. The variance of a Poisson distribution equals its mean value. We see that $\langle [\Delta N(T)]^2 \rangle \geq \langle N(T) \rangle$, with equality only when there is no excess noise, i.e., no randomness in $\{P(t) : 0 \leq t \leq T\}$, so that the photocount fluctuations are entirely due to shot noise. Light beams whose photocount variances fall below their mean photocounts are, therefore, said to be sub-Poissonian. Such beams are nonclassical, because their photocount statistics cannot be correctly described by semiclassical photodetection theory.

A second division between shot noise and excess noise appears in the photocurrent spectrum, when the illumination power $P(t)$ is a wide-sense stationary random process. In this case, $P(t)$ has a mean value $\langle P \rangle$ that is time-independent, a covariance function

$$K_{PP}(\tau) = \langle \Delta P(t + \tau) \Delta P(t) \rangle \quad (77)$$

that only depends on the time difference τ between the samples, and a noise spectral density

$$S_{PP}(\Omega) \equiv \int d\tau K_{PP}(\tau) e^{-j\Omega\tau}. \quad (78)$$

We then find that the photocurrent is also wide-sense stationary with constant mean

$$\langle i \rangle = \frac{q\eta\langle P \rangle}{\hbar\omega_0} \quad (79)$$

and noise spectral density [46]

$$S_{ii}(\Omega) = q\langle i \rangle + q^2\eta^2 S_{PP}(\Omega). \quad (80)$$

The first term on the right-hand side in (80) is the Schottky formula for the detector's shot noise, and the second term is the excess noise contributed by the power fluctuations in the illumination. Because noise spectra cannot be negative, we have $S_{ii}(\Omega) \geq q\langle i \rangle$, with equality at all frequencies only when there is no excess noise, i.e., no randomness in the illumination power. Light beams that give rise to subshot-noise photocurrent noise spectra are nonclassical, because their photocurrent statistics cannot be correctly described by semiclassical photodetection theory.

2) *Balanced Homodyne Detection:* Fig. 5 shows the configuration for balanced homodyne detection, as treated semi-classically. Here, the classical signal field $E_S(\rho, t)$ is combined on a 50–50 beam splitter with $E_{LO}(\rho, t)$, the field from a strong, continuous-wave (CW) local oscillator of the same frequency and polarization [47], [48]. The fields emerging from the beam splitter's output ports illuminate quantum efficiency η photodetectors, generating photocurrents whose difference is amplified and then filtered to extract the resulting baseband beat signal. For the moment, we will assume that the signal field is deterministic. We will take the local-oscillator field to

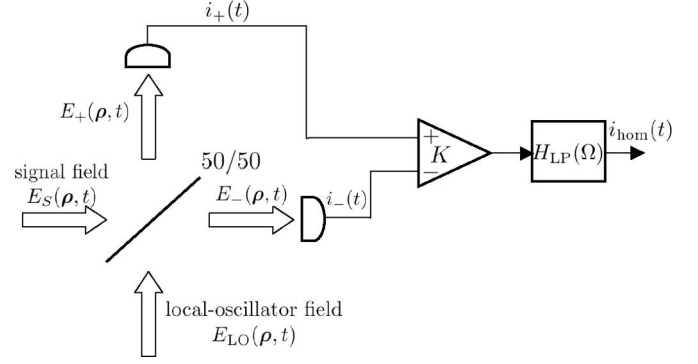


Fig. 5. Block diagram for balanced homodyne detection as treated in semiclassical photodetection theory.

be $E_{LO}(\rho, t) = \sqrt{P_{LO}/\hbar\omega_0} \phi_{LO}(\rho) e^{-j\omega_0 t}$, where $\phi_{LO}(\rho)$ for $\rho \in \mathcal{A}_d$ is its spatial mode and P_{LO} , its power, greatly exceeds $P_S(t)$, the short-time average signal power. The semiclassical statistics of balanced homodyne detection are easily developed from the results presented for direct detection. The positive-frequency fields $E_+(\rho, t)$ and $E_-(\rho, t)$ that illuminate the two photodetectors are given by

$$E_{\pm}(\rho, t) = \frac{E_S(\rho, t) \pm E_{LO}(\rho, t)}{\sqrt{2}}. \quad (81)$$

The photocurrents $i_+(t)$ and $i_-(t)$ are driven by short-time average powers

$$P_{\pm}(t) = \frac{P_{LO}}{2} \pm \sqrt{\hbar\omega_0 P_{LO}} \operatorname{Re} \left(\int_{\mathcal{A}_d} d^2\rho E_S(\rho, t) \phi_{LO}^*(\rho) e^{j\omega_0 t} \right) \quad (82)$$

where we have used $P_{LO} \gg P_S(t)$ to suppress a $P_S(t)/2$ term.

Writing each photocurrent as its mean $\langle i_{\pm}(t) \rangle$, plus its noise component $\Delta i_{\pm}(t)$, we have that the homodyne current has mean value

$$\begin{aligned} \langle i_{\text{hom}}(t) \rangle &= 2q\eta K \sqrt{\frac{P_{LO}}{\hbar\omega_0}} \\ &\times \int d\tau \operatorname{Re} \left(\int_{\mathcal{A}_d} d^2\rho E_S(\rho, \tau) \phi_{LO}^*(\rho) e^{j\omega_0 \tau} \right) h_{LP}(t - \tau) \end{aligned} \quad (83)$$

where $h_{LP}(t)$ is the impulse response associated with the ideal low-pass filter

$$H_{LP}(\Omega) = \begin{cases} 1, & \text{for } |\Omega| \leq \Omega_0 \\ 0, & \text{otherwise} \end{cases} \quad (84)$$

and noise component

$$\Delta i_{\text{hom}}(t) = K \int d\tau [\Delta i_+(\tau) - \Delta i_-(\tau)] h_{LP}(t - \tau). \quad (85)$$

When the low-pass filter $H_{LP}(\Omega)$ has sufficient bandwidth, we can simplify (83) to

$$\langle i_{\text{hom}}(t) \rangle = 2q\eta K \sqrt{\frac{P_{LO}}{\hbar\omega_0}} \times \text{Re} \left(\int_{\mathcal{A}_d} d^2\boldsymbol{\rho} E_S(\boldsymbol{\rho}, t) \phi_{LO}^*(\boldsymbol{\rho}) e^{j\omega_0 t} \right). \quad (86)$$

Because the shot noises from physically independent photodetectors are statistically independent random processes, and because the high rate-function limit of a filtered Poisson impulse train is a Gaussian random process [49], we have that $\Delta i_{\text{hom}}(t)$ is a zero-mean, stationary Gaussian random process with spectral density given by [50]

$$\mathcal{S}_{i_{\text{hom}} i_{\text{hom}}}(\Omega) = \frac{K^2 \eta q^2 P_{LO}}{\hbar\omega_0} |H_{LP}(\Omega)|^2. \quad (87)$$

Physically, $\langle i_{\text{hom}}(t) \rangle$ is proportional to the signal-field quadrature that is copolarized with and shares the same spatial mode and absolute phase as the local oscillator. For example, with $\phi_{LO}(\boldsymbol{\rho}) = e^{j\theta}/\sqrt{A_d}$, where A_d is the area of the \mathcal{A}_d pupil, we have that

$$\langle i_{\text{hom}}(t) \rangle = 2q\eta K \sqrt{\frac{P_{LO}}{\hbar\omega_0}} \times \text{Re} \left(\int_{\mathcal{A}_d} \frac{d^2\boldsymbol{\rho}}{\sqrt{A_d}} E_S(\boldsymbol{\rho}, t) e^{j(\omega_0 t - \theta)} \right) \quad (88)$$

which is proportional to the phase- θ quadrature of the normally incident plane-wave component of $E_S(\boldsymbol{\rho}, t)$ over \mathcal{A}_d .

According to semiclassical photodetection, the noise in the homodyne current is the white Gaussian shot noise of the strong local oscillator seen through the low-pass filter $H_{LP}(\Omega)$. If the signal field is not deterministic, its fluctuations will add noise to the homodyne current, as we saw earlier for direct detection. It follows that the minimum homodyne noise spectrum in semiclassical theory is given by the right-hand side of (87). Signal fields whose homodyne-current noise spectra fall below this local-oscillator shot-noise level are nonclassical, because their homodyne detection statistics cannot be correctly described by semiclassical photodetection theory.

3) *Balanced Heterodyne Detection:* Fig. 6 shows the configuration for balanced heterodyne detection, as treated semiclassically. It mimics what we have described for the homodyne case, but with two differences: the strong local-oscillator field is now at a radio frequency offset ω_{IF} , with IF denoting intermediate frequency, from the signal field, and the low-pass filter has been replaced by a bandpass filter centered at that intermediate frequency. It is now a very simple matter to establish the semiclassical theory of balanced heterodyne detection. Taking the local oscillator to be $E_{LO}(\boldsymbol{\rho}, t) = \sqrt{P_{LO}/\hbar\omega_0} \phi_{LO}(\boldsymbol{\rho}) e^{-j(\omega_0 - \omega_{IF})t}$, we can parallel the development for the homodyne case to show that the mean heterodyne current, when the ideal bandpass filter

$$H_{BP}(\Omega) = \begin{cases} 1, & \text{for } |\Omega \pm \omega_{IF}| \leq \Omega_0 \\ 0, & \text{otherwise} \end{cases} \quad (89)$$

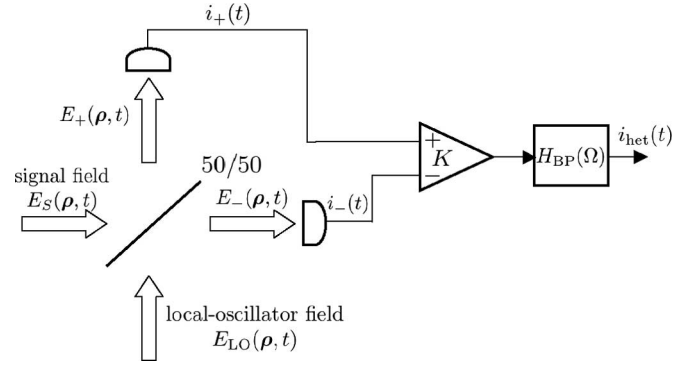


Fig. 6. Block diagram for balanced heterodyne detection as treated in semiclassical photodetection theory.

has sufficient bandwidth, is

$$\langle i_{\text{het}}(t) \rangle = 2q\eta K \sqrt{\frac{P_{LO}}{\hbar\omega_0}} \times \text{Re} \left(\int_{\mathcal{A}_d} d^2\boldsymbol{\rho} E_S(\boldsymbol{\rho}, t) \phi_{LO}^*(\boldsymbol{\rho}) e^{j(\omega_0 - \omega_{IF})t} \right). \quad (90)$$

For $E_S(\boldsymbol{\rho}, t) = A_S(\boldsymbol{\rho}, t) e^{-j\omega_0 t}$ and $\phi_{LO}(\boldsymbol{\rho}) = 1/\sqrt{A_d}$, this reduces to

$$\langle i_{\text{het}}(t) \rangle = 2q\eta K \sqrt{\frac{P_{LO}}{\hbar\omega_0}} \text{Re} \left(\int_{\mathcal{A}_d} \frac{d^2\boldsymbol{\rho}}{\sqrt{A_d}} A_S(\boldsymbol{\rho}, t) e^{-j\omega_{IF} t} \right) \quad (91)$$

which is proportional to the frequency downconverted—from ω_0 to ω_{IF} center frequency—version of the normally incident plane-wave component of the real-valued signal field $\text{Re}(A_S(\boldsymbol{\rho}, t) e^{-j\omega_0 t})$.

Assuming the signal field to be deterministic, the noise component of $i_{\text{het}}(t)$ is a zero-mean, stationary Gaussian random process with spectral density given by [50]

$$\mathcal{S}_{i_{\text{het}} i_{\text{het}}}(\Omega) = \frac{K^2 \eta q^2 P_{LO}}{\hbar\omega_0} |H_{BP}(\Omega)|^2 \quad (92)$$

i.e., it is the bandpass-filtered local-oscillator shot noise. As was the case for homodyne detection, any randomness in the signal field can only increase the noise in the heterodyne current, thus making the right-hand side of (92) the minimum heterodyne noise spectrum in semiclassical theory. Signal fields whose heterodyne current noise spectra fall below this local-oscillator shot-noise level are nonclassical, because their heterodyne detection statistics cannot be correctly described by semiclassical photodetection theory.

B. Quantum Theory

The quantum theory of photodetection has its roots in the multicoincidence rates introduced by Glauber [23], and the distinction between inclusive versus exclusive probabilities discussed by Kelley and Kleiner [51]. The development we shall present, however, relies on the quantum representation theorem for direct detection [8] (see also [47] and [48]).

1) *Direct Detection:* The photodetection phenomenology we discussed in Section III-A at the outset of our discussion

of semiclassical photodetection applies to the quantum case as well. Likewise, our quantum treatment will be limited to the statistical description for the photocurrent produced by an idealized detector with the following properties: its optical sensitivity covers all frequencies with constant efficiency $\eta \leq 1$; it has no dark current; it has no internal current multiplication; and its electrical bandwidth is infinite. What we need from a quantum theory of direct detection is then a prescription for going from the density operator $\hat{\rho}$ of $\hat{E}(\boldsymbol{\rho}, t)$, the $+z$ propagating, scalar, quasi-monochromatic, paraxial, positive-frequency field operator that illuminates the detector's photosensitive region, to the statistics of the classical photocurrent from (66). What quantum photodetection theory provides [8] is the equivalence between the statistics of this photocurrent, regarded as a classical random process, and the quantum measurement statistics of the photocurrent operator

$$\hat{i}(t) \equiv q \int_{\mathcal{A}_d} d^2 \boldsymbol{\rho} \hat{E}^{\dagger}(\boldsymbol{\rho}, t) \hat{E}'(\boldsymbol{\rho}, t) \quad (93)$$

where

$$\hat{E}'(\boldsymbol{\rho}, t) \equiv \sqrt{\eta} \hat{E}(\boldsymbol{\rho}, t) + \sqrt{1-\eta} \hat{E}_\eta(\boldsymbol{\rho}, t) \quad (94)$$

with $\hat{E}_\eta(\boldsymbol{\rho}, t)$ being a vacuum-state field operator arising from detector inefficiency whose δ -function commutator ensures that

$$[\hat{E}'(\boldsymbol{\rho}_1, t_1), \hat{E}'^{\dagger}(\boldsymbol{\rho}_2, t_2)] = \delta(\boldsymbol{\rho}_1 - \boldsymbol{\rho}_2) \delta(t_1 - t_2). \quad (95)$$

Equation (93) implies that the photocurrent $i(t)$ is equivalent to the electron charge multiplied by a measurement of the effective photon-flux operator, viz., the photon-flux operator for the field operator at the output of a fictitious beam splitter whose inputs are the field to be detected and a fictitious vacuum-state field. Equivalence between $i(t)$ and $\hat{i}(t)$ means that *all* statistics of the classical process are *identical* to the corresponding statistics of the quantum observable. In particular, the statistics of $i(t)$ are completely specified by the characteristic functional

$$M_i[jv(t)] \equiv \langle e^{j \int dt v(t) i(t)} \rangle \quad (96)$$

and the statistics of $\hat{i}(t)$ are completely specified by the characteristic functional

$$M_{\hat{i}}[jv(t)] \equiv \text{tr}(\hat{\rho} e^{j \int dt v(t) \hat{i}(t)}) \quad (97)$$

for $v(t)$ being an arbitrary real-valued waveform. According to (93), $M_i[jv(t)] = M_{\hat{i}}[jv(t)]$ for all $v(t)$.

Suppose that $\hat{E}(\boldsymbol{\rho}, t)$ is in the coherent state $|E(\boldsymbol{\rho}, t)\rangle$, i.e., it is a Gaussian state with

$$\langle \hat{E}(\boldsymbol{\rho}, t) \rangle = E(\boldsymbol{\rho}, t) \quad (98)$$

$$K_{EE}^{(n)}(\boldsymbol{\rho}_1, t_1; \boldsymbol{\rho}_2, t_2) = 0 \quad (99)$$

$$K_{EE}^{(p)}(\boldsymbol{\rho}_1, t_1; \boldsymbol{\rho}_2, t_2) = 0. \quad (100)$$

More simply, this state is an eigenket of $\hat{E}(\boldsymbol{\rho}, t)$ for all $(\boldsymbol{\rho}, t)$, with eigenfunction $E(\boldsymbol{\rho}, t)$, i.e., it is the spatiotemporal generalization of the photon annihilation operator's coherent state $|\alpha\rangle$. More importantly, when $\hat{E}(\boldsymbol{\rho}, t)$ is in the coherent state

$|E(\boldsymbol{\rho}, t)\rangle$, we find that

$$M_i[jv(t)] = \sum_{n=0}^{\infty} \frac{(\int dt e^{jqv(t)} \gamma(t))^n e^{-\int dt \gamma(t)}}{n!} \quad (101)$$

where

$$\gamma(t) \equiv \eta \int_{\mathcal{A}_d} d^2 \boldsymbol{\rho} |E(\boldsymbol{\rho}, t)|^2. \quad (102)$$

This characteristic functional coincides with that for the classical photocurrent $i(t)$ when its event times $\{t_n\}$ comprise a Poisson point process whose rate function $\gamma(t)$ is given by (102). Therefore, the quantum and semiclassical theories of direct detection predict *exactly* the same measurement statistics when the quantum field illuminating the photodetector is in a coherent state $|E(\boldsymbol{\rho}, t)\rangle$ whose eigenfunction equals the classical field that is employed in the semiclassical theory.

Now, suppose that $\hat{E}(\boldsymbol{\rho}, t)$ is in a mixed state with a proper P representation, i.e., a classically random mixture of coherent states $|E(\boldsymbol{\rho}, t)\rangle$ with different eigenfunctions. Conditioned on knowledge of the coherent-state eigenfunction, the photocurrent's characteristic functional in quantum photodetection will be as given in the preceding paragraph. It follows that the unconditional photocurrent characteristic functional for the $0 \leq t \leq T$ time interval is found by averaging (101) over the randomness in the coherent-state eigenfunction

$$M_i[jv(t)] = \left\langle \sum_{n=0}^{\infty} \frac{(\int d\tau e^{jqv(\tau)} \gamma(\tau))^n e^{-\int d\tau \gamma(\tau)}}{n!} \right\rangle. \quad (103)$$

However, the P function for this state is nothing more or less than the statistics of a classical random process $E(\boldsymbol{\rho}, t)$. So, if we use semiclassical photodetection theory with these statistics for a random classical illumination $E(\boldsymbol{\rho}, t)$, we will get *exactly* the same characteristic functional for $i(t)$ as we have just found via the quantum approach. In short, for illumination that is a classically random mixture of coherent states, *all* statistics obtained from quantum photodetection theory coincide with those obtained from the semiclassical treatment. For that reason, we say that classically random mixtures of coherent states are *classical* states; all other states are deemed to be nonclassical in that at least some of their photodetection statistics defy semiclassical explanation, as we shall see shortly.

To illustrate what can happen in direct detection with nonclassical light, suppose that the only excited mode in $\hat{E}(\boldsymbol{\rho}, t)$ is $e^{-j\omega_0 t} / \sqrt{A_d T}$ for $\boldsymbol{\rho} \in \mathcal{A}_d$ and $0 \leq t \leq T$, and that this mode is in the N -photon Fock state $|N\rangle$ with $N > 0$.³ It is then straightforward to show that

$$\hat{N}(T) \equiv \frac{1}{q} \int_0^T dt \hat{i}(t) \quad (104)$$

has the binomial distribution

$$\Pr(N(T) = n) = \binom{N}{n} \eta^n (1-\eta)^{N-n} \quad \text{for } 0 \leq n \leq N \quad (105)$$

³Fock states, coherent states, and squeezed states are arguably the three most significant light-beam quantum states. Whereas the latter two are Gaussian states, the Fock state is not.

where $N(T)$ is the classical outcome of the $\hat{N}(T)$ measurement. This distribution is sub-Poissonian for all $0 < \eta \leq 1$, because its variance is less than its mean

$$\langle [\Delta N(T)]^2 \rangle = N\eta(1 - \eta) < N\eta = \langle N(T) \rangle \quad (106)$$

which is something that cannot occur in semiclassical photodetection.

2) *Balanced Homodyne Detection*: The block diagram for balanced homodyne detection in the quantum theory is the semiclassical arrangement shown in Fig. 5 with field operators $\hat{E}_S(\rho, t)$ and $\hat{E}_{LO}(\rho, t)$ replacing the classical fields shown in that figure. The former may be in an arbitrary quantum state, but the latter is in the coherent state $|\sqrt{P_{LO}/\hbar\omega_0} \phi_{LO}(\rho) e^{-j\omega_0 t}\rangle$, with

$$P_{LO} \gg \int_{\mathcal{A}_d} d^2\rho \langle \hat{E}_S^\dagger(\rho, t) \hat{E}_S(\rho, t) \rangle \quad (107)$$

providing the strong local-oscillator condition. It is shown in [8] that the homodyne current $i_{\text{hom}}(t)$ is a classical random process whose statistics coincide with those of the following homodyne-current operator:

$$\begin{aligned} \hat{i}_{\text{hom}}(t) &= 2qK \sqrt{\frac{\eta P_{LO}}{\hbar\omega_0}} \\ &\times \int d\tau \operatorname{Re} \left(\int_{\mathcal{A}_d} d^2\rho \hat{E}'_S(\rho, \tau) \phi_{LO}^*(\rho) e^{j\omega_0 \tau} \right) \\ &\times h_{LP}(t - \tau) \end{aligned} \quad (108)$$

where

$$\hat{E}'_S(\rho, t) \equiv \sqrt{\eta} \hat{E}_S(\rho, t) + \sqrt{1 - \eta} \hat{E}_\eta(\rho, t). \quad (109)$$

Specializing to $\phi_{LO}(\rho) = e^{j\theta}/\sqrt{A_d}$ gives $\hat{i}_{\text{hom}}(t)$ being proportional to the phase- θ quadrature of the normally incident plane-wave component of $\hat{E}'_S(\rho, t)$ over \mathcal{A}_d with frequency content within $\pm\Omega_0$ of ω_0 .

Equation (108) is a remarkable result that stands in stark contrast to what we have seen for the semiclassical case, in which the fundamental homodyne-current noise is local-oscillator shot noise. In the quantum theory of balanced homodyne detection, the coherent-state local oscillator does *not* contribute to the homodyne-current noise, which is entirely due to the noise in the effective field operator $\hat{E}'_S(\rho, t)$. Nevertheless, this disparity of noise interpretation does *not* preclude both theories agreeing quantitatively when the signal field is in a coherent state, as we will now show. The same concurrence is found when $\hat{E}_S(\rho, t)$ is in a classical state; the proof follows the argument given earlier for direct detection.

Assume that $\hat{E}_S(\rho, t)$ is in the coherent state $|E_S(\rho, t)\rangle$. Because $\hat{E}_\eta(\rho, t)$ is in its vacuum state, which itself is a coherent state, it is easily shown that $\hat{E}'_S(\rho, t)$ is in the coherent state $|\sqrt{\eta} E_S(\rho, t)\rangle$, from which it follows that the $\hat{i}_{\text{hom}}(t)$ measurement yields a classical Gaussian random process $i_{\text{hom}}(t)$

consisting of a mean

$$\begin{aligned} \langle i_{\text{hom}}(t) \rangle &= 2q\eta K \sqrt{\frac{P_{LO}}{\hbar\omega_0}} \\ &\times \int d\tau \operatorname{Re} \left(\int_{\mathcal{A}_d} d^2\rho E_S(\rho, \tau) \phi_{LO}^*(\rho) e^{j\omega_0 \tau} \right) \\ &\times h_{LP}(t - \tau) \end{aligned} \quad (110)$$

plus a noise component $\Delta i_{\text{hom}}(t)$ that is a zero-mean stationary random process with spectral density

$$\mathcal{S}_{i_{\text{hom}} i_{\text{hom}}}(\Omega) = \frac{K^2 \eta q^2 P_{LO}}{\hbar\omega_0} |H_{LP}(\Omega)|^2. \quad (111)$$

Comparison of (110) and (111) with (83) and (87) demonstrates that coherent-state illumination $|E_S(\rho, t)\rangle$ leads to the same statistics for homodyne detection in the quantum theory of photodetection that semiclassical theory does for deterministic illumination $E_S(\rho, t)$.

To illustrate what can happen in balanced homodyne detection with nonclassical light, suppose that $\hat{E}_S(\rho, t)$ is in a single spatial-mode squeezed-vacuum state, specifically, the zero-mean Gaussian state with the following covariance functions

$$\begin{aligned} K_{E_S E_S}^{(n)}(\rho_1, t_1; \rho_2, t_2) &= \int \frac{d\Omega}{2\pi} \frac{|\nu(\Omega)|^2}{A_d} e^{j\Omega(t_1 - t_2)} \\ &\times e^{j\omega_0(t_1 - t_2)} \end{aligned} \quad (112)$$

$$\begin{aligned} K_{E_S E_S}^{(p)}(\rho_1, t_1; \rho_2, t_2) &= \int \frac{d\Omega}{2\pi} \frac{\mu(\Omega)\nu(\Omega)}{A_d} e^{j\Omega(t_1 - t_2)} \\ &\times e^{-j\omega_0(t_1 + t_2)} \end{aligned} \quad (113)$$

for $\rho_1, \rho_2 \in \mathcal{A}_d$, where $|\mu(\Omega)|^2 - |\nu(\Omega)|^2 = 1$. The resulting homodyne-current noise spectrum when $\phi_{LO}(\rho) = e^{j\theta}/\sqrt{A_d}$ turns out to be

$$\begin{aligned} \mathcal{S}_{i_{\text{hom}} i_{\text{hom}}}(\Omega) &= \frac{K^2 \eta q^2 P_{LO}}{\hbar\omega_0} |H_{LP}(\Omega)|^2 \\ &\times [(1 - \eta) + \eta(|\mu(\Omega)| + \nu^*(\Omega)e^{j\theta})^2] \end{aligned} \quad (114)$$

where the $(1 - \eta)$ term in the bracket is due to the θ -quadrature vacuum-state quantum noise in $\hat{E}_\eta(\rho, t)$, and the $\eta|\mu(\Omega)| + \nu^*(\Omega)e^{j\theta}|^2$ term in that bracket is due to the θ -quadrature squeezed-state quantum noise in $\hat{E}_S(\rho, t)$. For θ such that the homodyne detector is measuring the low-noise quadrature of this squeezed state at frequency Ω , we get

$$\begin{aligned} \mathcal{S}_{i_{\text{hom}} i_{\text{hom}}}(\Omega) &= \frac{K^2 \eta q^2 P_{LO}}{\hbar\omega_0} |H_{LP}(\Omega)|^2 \\ &\times [(1 - \eta) + \eta(|\mu(\Omega)| - |\nu(\Omega)|)^2]. \end{aligned} \quad (115)$$

Because

$$(|\mu(\Omega)| - |\nu(\Omega)|)^2 = \frac{1}{(|\mu(\Omega)| + |\nu(\Omega)|)^2} < 1 \quad (116)$$

when $|\nu(\Omega)| > 0$, the homodyne noise spectrum obtained for the squeezed state's low-noise quadrature is *below* the local-oscillator shot-noise limit. Hence, it cannot be accounted for by semiclassical photodetection theory.

3) *Balanced Heterodyne Detection*: The block diagram for balanced heterodyne detection in the quantum theory is the Fig. 6 setup with field operators $\hat{E}(\boldsymbol{\rho}, t)$ and $\hat{E}_{\text{LO}}(\boldsymbol{\rho}, t)$ replacing the classical fields $E_S(\boldsymbol{\rho}, t)$ and $E_{\text{LO}}(\boldsymbol{\rho}, t)$. We will take $\hat{E}(\boldsymbol{\rho}, t)$ to be in a quantum state whose excited (nonvacuum) temporal modes lie within $\pm\Omega_0$ of ω_0 , but is otherwise arbitrary, while we will assume that $\hat{E}_{\text{LO}}(\boldsymbol{\rho}, t)$ is in the coherent state $|\sqrt{P_{\text{LO}}/\hbar\omega_0}\phi_{\text{LO}}(\boldsymbol{\rho})e^{-j(\omega_0-\omega_{\text{IF}})t}\rangle$, with

$$P_{\text{LO}} \gg \int_{\mathcal{A}_d} d^2\boldsymbol{\rho} \langle \hat{E}^\dagger(\boldsymbol{\rho}, t) \hat{E}(\boldsymbol{\rho}, t) \rangle \quad (117)$$

providing the strong local-oscillator condition. We shall also assume that the frequency components of $\hat{E}(\boldsymbol{\rho}, t)$ within $\pm\Omega_0$ of $\omega_0 - 2\omega_{\text{IF}}$ are all unexcited. This condition allows us to identify two finite-bandwidth field operators, $\hat{E}_S(\boldsymbol{\rho}, t)$ and $\hat{E}_I(\boldsymbol{\rho}, t)$, whose beat notes with the local-oscillator field will produce outputs in the passband of $H_{\text{BP}}(\Omega)$. The former is the signal-band (S) field, which contains the modes in the frequency range $|\omega - \omega_0| \leq \Omega_0$. The latter is the image-band (I) field [52], which is composed entirely of unexcited modes in the frequency range $|\omega + 2\omega_{\text{IF}} - \omega_0| \leq \Omega_0$. In semiclassical photodetection, the unexcited image-band field makes no contribution to the heterodyne current, but in the quantum theory this unexcited image band contributes quantum noise to that current. From [8], we have that the heterodyne current $i_{\text{het}}(t)$ is a classical random process whose statistics are identical to those of the heterodyne-current operator $\hat{i}_{\text{het}}(t)$, given by

$$\begin{aligned} \hat{i}_{\text{het}}(t) = & 2qK \sqrt{\frac{\eta P_{\text{LO}}}{\hbar\omega_0}} \\ & \times \text{Re} \left(\int_{\mathcal{A}_d} d^2\boldsymbol{\rho} [\hat{E}'_S(\boldsymbol{\rho}, t) + \hat{E}'_I(\boldsymbol{\rho}, t)] \phi_{\text{LO}}^*(\boldsymbol{\rho}) \right. \\ & \left. \times e^{j(\omega_0 - \omega_{\text{IF}})t} \right) \end{aligned} \quad (118)$$

where

$$\hat{E}'_K(\boldsymbol{\rho}, t) \equiv \sqrt{\eta} \hat{E}_K(\boldsymbol{\rho}, t) + \sqrt{1-\eta} \hat{E}_{\eta_K}(\boldsymbol{\rho}, t) \quad (119)$$

for $K = S, I$, with $\{\hat{E}_{\eta_K}(\boldsymbol{\rho}, t)\}$ being a pair of vacuum-state field operators—with the same frequency content as $\{\hat{E}_K(\boldsymbol{\rho}, t)\}$ —that account for the detector's quantum efficiency.

To develop a more informative expression for $\hat{i}_{\text{het}}(t)$, let us assume that $\phi_{\text{LO}}(\boldsymbol{\rho}) = 1/\sqrt{A_d}$ for $\boldsymbol{\rho} \in \mathcal{A}_d$, and introduce the set of baseband field operators defined by

$$\hat{A}_S(t) \equiv \int_{\mathcal{A}_d} \frac{d^2\boldsymbol{\rho}}{\sqrt{A_d}} \hat{E}_S(\boldsymbol{\rho}, t) e^{j\omega_0 t} \quad (120)$$

$$\hat{A}_{\eta_S}(t) \equiv \int_{\mathcal{A}_d} \frac{d^2\boldsymbol{\rho}}{\sqrt{A_d}} \hat{E}_{\eta_S}(\boldsymbol{\rho}, t) e^{j\omega_0 t} \quad (121)$$

$$\hat{A}_I(t) \equiv \int_{\mathcal{A}_d} \frac{d^2\boldsymbol{\rho}}{\sqrt{A_d}} \hat{E}_I(\boldsymbol{\rho}, t) e^{j(\omega_0 - 2\omega_{\text{IF}})t} \quad (122)$$

$$\hat{A}_{\eta_I}(t) \equiv \int_{\mathcal{A}_d} \frac{d^2\boldsymbol{\rho}}{\sqrt{A_d}} \hat{E}_{\eta_I}(\boldsymbol{\rho}, t) e^{j(\omega_0 - 2\omega_{\text{IF}})t}. \quad (123)$$

The heterodyne-current operator from (118) then reduces to

$$\begin{aligned} \hat{i}_{\text{het}}(t) = & 2qK \sqrt{\frac{\eta P_{\text{LO}}}{\hbar\omega_0}} [\text{Re}(\sqrt{\eta}[\hat{A}_S(t) + \hat{A}_I^\dagger(t)]e^{-j\omega_{\text{IF}}t}) \\ & + \text{Re}(\sqrt{1-\eta}[\hat{A}_{\eta_S}(t) + \hat{A}_{\eta_I}^\dagger(t)]e^{-j\omega_{\text{IF}}t})]. \end{aligned} \quad (124)$$

If $\hat{E}_S(\boldsymbol{\rho}, t)$ is in the coherent state $|E_S(\boldsymbol{\rho}, t)\rangle$, where

$$A_S(t) = \int_{\mathcal{A}_d} \frac{d^2\boldsymbol{\rho}}{\sqrt{A_d}} E_S(\boldsymbol{\rho}, t) e^{j\omega_0 t} \quad (125)$$

then (124) implies that the classical random-process heterodyne current will be a Gaussian random process with mean

$$\langle \hat{i}_{\text{het}}(t) \rangle = 2q\eta K \sqrt{\frac{P_{\text{LO}}}{\hbar\omega_0}} \text{Re}(A_S(t) e^{-j\omega_{\text{IF}}t}) \quad (126)$$

plus a noise component $\Delta i_{\text{het}}(t)$ that is a zero-mean, stationary Gaussian random process with spectral density

$$\mathcal{S}_{i_{\text{het}} i_{\text{het}}}(\Omega) = \frac{K^2 \eta^2 P_{\text{LO}}}{\hbar\omega_0} |H_{\text{BP}}(\Omega)|^2. \quad (127)$$

These results coincide with what we found using semiclassical analysis: see (91) with $A_S(\boldsymbol{\rho}, t) = A_S(t)/\sqrt{A_d}$ and (92). Furthermore, as we saw earlier for direct detection, the agreement between the semiclassical and quantum theories of balanced heterodyne detection also occurs when the signal field is in a classical state. This quantitative agreement, for classical-state light, contrasts with the difference in physical interpretation of the noise origin. The semiclassical theory asserts that local-oscillator shot noise is the fundamental noise in heterodyne detection, whereas the quantum theory teaches that it is the quantum noise from the signal band, the image band, and the loss associated with subunity detector quantum efficiency.

Our final task, in reviewing quantum photodetection theory, will be to show that *only* classical states yield photodetection statistics that agree with semiclassical predictions in all three basic detection modalities, i.e., direct detection, homodyne detection, and heterodyne detection. We have already given examples of nonclassical states that violate the semiclassical descriptions of direct and homodyne detection. To prove our assertion that a nonclassical state must violate some prediction of semiclassical photodetection, we build upon what we have just established for the quantum theory of heterodyne detection. Moreover, for simplicity, we shall limit our consideration to a single excited mode; the generalization of this proof to the full field operator merely entails more complicated tensor-product notation.

Without loss of generality, we can assume that the detectors have unity quantum efficiency, so that

$$\hat{i}_{\text{het}}(t) = 2qK \sqrt{\frac{P_{\text{LO}}}{\hbar\omega_0}} \text{Re}([\hat{A}_S(t) + \hat{A}_I^\dagger(t)]e^{-j\omega_{\text{IF}}t}). \quad (128)$$

If $e^{-j\omega_0 t}/\sqrt{T}$ for $0 \leq t \leq T$ with $\omega_{\text{IF}}T \gg 1$ is the excited mode of $\hat{A}_S(t)e^{-j\omega_0 t}$, then

$$\frac{\int_0^T dt \hat{i}_{\text{het}}(t) e^{j\omega_{\text{IF}}t}}{4qK \sqrt{P_{\text{LO}}T/\hbar\omega_0}} = \hat{a}_S + \hat{a}_I^\dagger. \quad (129)$$

Here,

$$\hat{a}_K \equiv \int_0^T \frac{dt}{\sqrt{T}} \hat{A}_K(t), \quad \text{for } K = S, I \quad (130)$$

are the photon annihilation operators for the excited signal-band mode (S) and the relevant vacuum-state image-band mode (I). The classical outcome from this measurement, given by

$$\alpha_S \equiv \frac{\int_0^T dt i_{\text{het}}(t) e^{j\omega_{\text{IF}} t}}{4qK \sqrt{P_{\text{LO}} T / \hbar \omega_0}} \quad (131)$$

is a complex-valued random variable, $\alpha_S = \alpha_{S_1} + j\alpha_{S_2}$, whose joint probability density is known to be [53]

$$p(\alpha_S) = \frac{\langle \alpha_S | \hat{\rho}_S | \alpha_S \rangle}{\pi} \quad (132)$$

where $|\alpha_S\rangle$ is the coherent state of the \hat{a}_S mode and $\hat{\rho}_S$ is the density operator of that mode. The statistics of heterodyne detection, therefore, determine the density operator, because the antinormally ordered characteristic function of $\hat{\rho}_S$ can be found from

$$\chi_A^{\rho_S}(\zeta^*, \zeta) = \int d^2 \alpha_S p(\alpha_S) e^{-\zeta^* \alpha_S + \zeta \alpha_S^*} \quad (133)$$

from which the density operator itself can be retrieved via the operator-valued inverse Fourier transform

$$\hat{\rho}_S = \int \frac{d^2 \zeta}{\pi} \chi_A^{\rho_S}(\zeta^*, \zeta) e^{-\zeta \hat{a}^\dagger} e^{\zeta^* \hat{a}}. \quad (134)$$

Under the same conditions assumed in the preceding paragraph, the semiclassical theory of heterodyne detection predicts that the observation will satisfy

$$\alpha_S = a_S + n_{\text{LO}} \quad (135)$$

where a_S is the classical phasor of the signal mode being detected and n_{LO} —the local-oscillator shot noise contribution to α_S —is a zero-mean, isotropic, complex-valued Gaussian random variable with $\langle |n_{\text{LO}}|^2 \rangle = 1$. Using the semiclassical $p(\alpha_S)$ to calculate $\langle e^{-\zeta^* \alpha_S} e^{\zeta \alpha_S^*} \rangle$ —the semiclassical version of (133)—and retrieving a density operator from the semiclassical version of (134), i.e.,

$$\hat{\rho}_S = \int \frac{d^2 \zeta}{\pi} \langle e^{-\zeta^* \alpha_S} e^{\zeta \alpha_S^*} \rangle e^{-\zeta \hat{a}^\dagger} e^{\zeta^* \hat{a}} \quad (136)$$

then gives

$$\hat{\rho}_S = \int d^2 a_S p(a_S) |a_S\rangle \langle a_S| \quad (137)$$

where $p(a_S)$ is the joint probability density for the real and imaginary parts of the classical signal-field phasor a_S and $|a_S\rangle$ is the coherent state of the \hat{a}_S mode with eigenvalue a_S . This density operator is a classical state, because (137) with $p(a_S)$ a probability density is a proper P representation, i.e., $\hat{\rho}_S$ is a classically random mixture of coherent states $|a_S\rangle$ with probability density $p(a_S)$.

In summary, the statistics of heterodyne detection found from quantum theory determine the density operator of the signal

field, and *only* if this density operator has a proper P representation can these heterodyne statistics be consistent with the semiclassical theory of heterodyne detection.

C. Coincidence Counting on Entangled Gaussian States

SPDC in a second-order nonlinear crystal is the primary source for entangled, or even hyper-entangled, photon pairs [12], [27]. Photon-coincidence counting is the primary means by which the entanglement in these pairs is verified, and also the technique by which their entanglement is exploited in applications such as qubit teleportation [15], quantum optical coherence tomography [54], and quantum ghost imaging [55]. In most SPDC analyses and experiments, the joint state of the signal and idler beams—after a postselection procedure that only includes photon coincidences—is modeled as a biphoton wave packet. For CW operation at frequency degeneracy of a type-II phase-matched downconverter, with fiber couplers used to restrict attention to single spatial modes of the signal and idler beams, the maximally entangled biphoton wave packet takes the form of a twin-beam (TB) state [56]

$$|\text{TB}\rangle \equiv \int \frac{d\omega}{2\pi} j\kappa A_P \ell \frac{\sin(\omega \Delta k' \ell / 2)}{\omega \Delta k' \ell / 2} |\omega_P / 2 + \omega\rangle_S |\omega_P / 2 - \omega\rangle_I \quad (138)$$

where $\text{Re}(A_P e^{-j\omega_P t})$ is the single spatial-mode pump field with photon flux $|A_P|^2$ and frequency ω_P , $|\omega_P / 2 + \omega\rangle_S$ denotes a single photon of the signal beam's excited polarization at frequency $\omega_P / 2 + \omega$, $|\omega_P / 2 - \omega\rangle_I$ denotes a single photon of the idler beam's excited polarization at frequency $\omega_P / 2 - \omega$, κ is the nonlinear coupling constant, ℓ is the crystal length, and $\sin(\omega \Delta k' \ell / 2) / (\omega \Delta k' \ell / 2)$ gives the phase-matching function in terms of the frequency derivative of the wavenumber mismatch, $\Delta k(\omega) \equiv k_P(\omega_P) - k_S(\omega_P / 2 + \omega) - k_I(\omega_P / 2 - \omega)$, at zero detuning, $\omega = 0$. Equation (138) also assumes that a post-SPDC compensating crystal has been employed to compensate for the group velocity difference between the orthogonally polarized signal and idler beams.

The TB state is entangled in frequency, but its signal and idler components have definite polarizations. If two of the preceding type-II downconverters are coherently pumped and their outputs combined appropriately, we can obtain the frequency-entangled polarization singlet state [57]

$$\begin{aligned} |\psi^-\rangle &= \int \frac{d\omega}{2\pi} j\kappa A_P \ell \frac{\sin(\omega \Delta k' \ell / 2)}{\omega \Delta k' \ell / 2} \\ &\times (|\omega_P / 2 + \omega\rangle_{S_x} |\omega_P / 2 - \omega\rangle_{I_y} \\ &- |\omega_P / 2 + \omega\rangle_{S_y} |\omega_P / 2 - \omega\rangle_{I_x}) \end{aligned} \quad (139)$$

with the obvious notation for the x and y polarizations of $+z$ -propagating signal and idler beams.

Neither the TB state nor the frequency-entangled singlet state is properly normalized: Their definitions lead to $\langle \text{TB} | \text{TB} \rangle = \infty$ and $\langle \psi^- | \psi^- \rangle = \infty$. Moreover, CW SPDC produces an infinite stream of photon pairs; therefore, (138) and (139) are useful only when the photodetection interval is short enough that it will contain one pair at most. These issues are easily circumvented for CW SPDC without pump depletion, because the

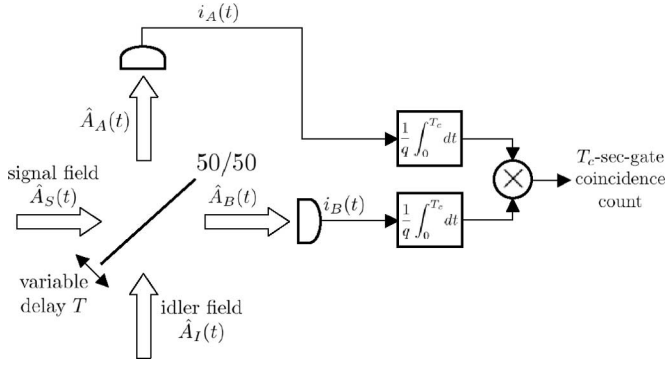


Fig. 7. Block diagram of the HOM interferometer.

signal and idler outputs from such a source are in a zero-mean jointly Gaussian state [27], and hence, characterized by their autocorrelations and cross-correlations.⁴ In the rest of this section, we shall use the Gaussian-state characterization to demonstrate the photon-coincidence dip seen in HOM interferometry when the input fields come from one downconverter, and the violation of the CHSH inequality when the input fields are the coherently combined outputs from a pair of coherently pumped downconverters. Apart from its being an illustrative application of Gaussian-state analysis, the study in this section rigorously accounts for the multiple-pair events that are handled in an *ad hoc* fashion by theorists who use the biphoton state to analyze coincidence-counting measurements, and referred to as “accidental” coincidences by the experimentalists who perform such measurements.

1) HOM Interferometry: Fig. 7 shows the HOM interferometer [30] with the signal and idler beams from a CW SPDC source as its inputs. In order that these beams interfere at the 50–50 beam splitter in Fig. 7, the idler beam’s polarization is rotated by 90° by a half-wave plate (HWP) (not shown), so that signal and idler are copolarized when they reach the beam splitter. The outputs from the beam splitter then illuminate a pair of photodetectors, whose photocount coincidences, over a T_c -second-long coincidence window, are registered and averaged. With $\hat{A}_K(t)e^{-j\omega_P t/2}/\sqrt{A_d}$, for $\rho \in A_d$ and $K = S, I$, denoting the single excited spatial modes of the copolarized signal and idler arriving at the beam splitter, it follows from [27] that the baseband field operators $\hat{A}_S(t)$ and $\hat{A}_I(t)$ are in a statistically stationary, zero-mean, jointly Gaussian state with the following nonzero covariance functions:

$$K_{A_S A_S}^{(n)}(\tau) = K_{A_I A_I}^{(n)}(\tau) = K^{(n)}(\tau) \quad (140)$$

$$\equiv \begin{cases} \frac{|\kappa A_P|^2 \ell}{|\Delta k'|} \left(1 - \left|\frac{\tau}{\Delta k' \ell}\right|\right), & \text{for } |\tau| \leq |\Delta k' \ell| \\ 0, & \text{otherwise} \end{cases} \quad (141)$$

⁴For pulse-pumped SPDC, biphoton analysis does not encounter a normalization problem [58], but that treatment ignores the higher order (multiple-pair) terms in the full Gaussian-state analysis of downconversion.

for $K = S, I$, and

$$K_{A_S A_I}^{(p)}(\tau) = \begin{cases} j\kappa A_P / |\Delta k'|, & \text{for } |\tau| \leq |\Delta k' \ell|/2 \\ 0, & \text{otherwise.} \end{cases} \quad (142)$$

The baseband field operators for the single spatial-mode illumination impinging on the photodetectors in Fig. 7 are

$$\hat{A}_A(t) = \frac{\hat{A}_S(t) + \hat{A}_I(t - T/2)}{\sqrt{2}} \quad (143)$$

$$\hat{A}_B(t) = \frac{\hat{A}_S(t + T/2) - \hat{A}_I(t)}{\sqrt{2}} \quad (144)$$

where T is a variable time delay that is set by moving the beam splitter. Inasmuch as these fields are a linear transformation of the signal and idler, they too are in a statistically stationary, zero-mean, jointly Gaussian state. This state is specified by the nonzero covariance functions

$$K_{A_A A_A}^{(n)}(\tau) = K_{A_B A_B}^{(n)}(\tau) = K^{(n)}(\tau) \quad (145)$$

$$K_{A_A A_B}^{(p)}(\tau) = \frac{-K_{A_S A_I}^{(p)}(\tau) + K_{A_S A_I}^{(p)}(T - \tau)}{2}. \quad (146)$$

To complete our Gaussian-state analysis of the HOM coincidence dip seen with CW SPDC light, we employ the state we have just characterized with our quantum theory of photodetection.

Suppose that

$$\hat{N}_K(T_c; T) \equiv \frac{1}{q} \int_0^{T_c} dt \hat{i}_K(t), \quad \text{for } K = A, B \quad (147)$$

are the T_c -second-interval photocount operators for detectors A and B in Fig. 7 when the beam splitter delay is set to T . If the SPDC photon flux is sufficiently low for the chosen T_c value, then, with high probability, at most one count will occur on each detector, and we can use

$$C(T_c; T) \equiv \langle \hat{N}_A(T_c; T) \hat{N}_B(T_c; T) \rangle \quad (148)$$

$$= \frac{1}{q^2} \int_0^{T_c} dt \int_0^{T_c} du \langle \hat{i}_A(t) \hat{i}_B(u) \rangle \quad (149)$$

$$= \eta^2 \int_0^{T_c} dt \int_0^{T_c} du \langle \hat{A}_A^\dagger(t) \hat{A}_A(t) \hat{A}_B^\dagger(u) \hat{A}_B(u) \rangle \quad (150)$$

as the ensemble-average value of the HOM interferometer’s coincidence count. Applying Gaussian-state moment factoring [see (65)], we find that

$$C(T_c; T) = (\eta K^{(n)}(0) T_c)^2 + \eta^2 T_c \int_{-T_c}^{T_c} d\tau \left(1 - \frac{|\tau|}{T_c}\right) |K_{A_A A_B}^{(p)}(\tau)|^2. \quad (151)$$

Expressing the \hat{A}_A and \hat{A}_B covariances in terms of those given before for \hat{A}_S and \hat{A}_I , and noting that SPDC coherence times (reciprocal phase-matching bandwidths) are short, $|\Delta k' \ell| \sim \text{ps}$, in comparison to coincidence-counting intervals, $T_c \sim \text{ns}$, we

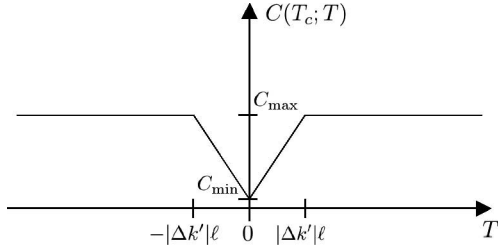


Fig. 8. Average coincidence count $C(T_c; T)$ versus delay T for a type-II phase-matched SPDC source: $C_{\min} = (2\eta PT_c/\hbar\omega_P)^2$ and $C_{\max} = (2\eta PT_c/\hbar\omega_P)^2 + \eta^2 PT_c/\hbar\omega_P$.

can reduce (150) to

$$C(T_c; T) = \begin{cases} \left(\frac{\eta PT_c}{\hbar\omega_P/2} \right)^2 + \frac{\eta^2 PT_c |T|}{\hbar\omega_P |\Delta k'| \ell}, & \text{for } |T| \leq |\Delta k'| \ell \\ \left(\frac{\eta PT_c}{\hbar\omega_P/2} \right)^2 + \frac{\eta^2 PT_c}{\hbar\omega_P}, & \text{for } |\Delta k'| \ell < |T| \ll T_c \end{cases} \quad (152)$$

where $P \equiv |\kappa A_P|^2 \ell / |\Delta k'|$ is the downconverter's photon-pair flux, i.e., the number of signal (and idler) photons it emits per second into the spatial mode under consideration. The plot of $C(T_c; T)$ versus T in Fig. 8 reveals the main features of an HOM interference measurement on the SPDC-produced, maximally entangled, jointly Gaussian state of the signal and idler. The first term in (152) is the so-called accidental coincidences that set the minimum value of $C(T_c; T)$. It equals the average number of counts on detector A multiplied by the average number of counts on detector B . Added to this constant baseline is the familiar triangular HOM dip. Its minimum at zero delay ($T = 0$) occurs because the signal and idler photons arriving at the beam splitter are then indistinguishable; hence, quantum interference leads both to exit from the same output port. As T is increased, the time shift between the signal and idler photons arriving at the beam splitter makes them increasingly distinguishable, thus increasing the probability that one will exit from each of the beam splitter's output ports. Our low-flux assumption implies that $2\eta PT_c/\hbar\omega_P \ll 1$, thus making the average coincidence count—when $|\Delta k'| \ell < |T| \ll T_c$ —much greater than the accidental level for reasonable values of the quantum efficiency η . Thus, the dip at $T = 0$ is quite pronounced. The HOM dip is an interference phenomenon that is fourth order in the field operators, but, because we are considering Gaussian states, this fourth-order interference was evaluated from second-order field moments. It is a *nonclassical* interference phenomenon, because, as shown in [41], classical signal fields $A_S(t)$ and $A_I(t)$ that are zero-mean, jointly Gaussian random processes will lead to a miniscule dip in the average coincidence count at zero delay.

2) *CHSH Inequality*: The CHSH inequality [31] is a variant of Bell's inequality [59] that is routinely used to show that polarization-entangled photon pairs obtained from SPDC have quantum interference behavior that cannot be explained

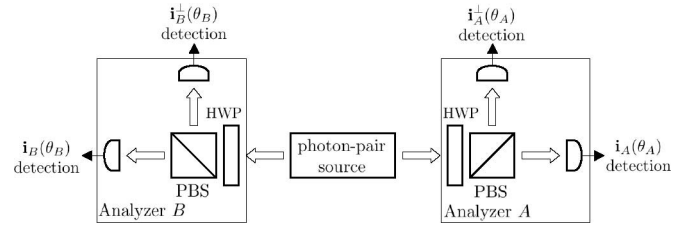


Fig. 9. Setup for testing the CHSH inequality: polarizing beam splitter (PBS).

by local hidden variables.⁵ We will begin by briefly reviewing the standard derivation of the inequality and how it is violated by the polarization-qubit singlet state. Then, we shall show how the CHSH violation is demonstrated with the frequency- and polarization-entangled light obtained from a pair of coherently pumped CW downconverters.

The conceptual setup for testing the CHSH inequality—under ideal conditions—is shown in Fig. 9. The source in this figure produces a photon pair, sending one to polarization analyzer A and the other to polarization analyzer B . Each analyzer consists of an HWP, a polarizing beam splitter, and a pair of unity-quantum-efficiency photon counters. Thus, in analyzer $K = A, B$, one and only one detector will click, indicating that a photon has been observed that is polarized along the unit vector

$$\mathbf{i}_K(\theta_K) \equiv \cos(\theta_K) \mathbf{i}_x + \sin(\theta_K) \mathbf{i}_y \quad (153)$$

or

$$\mathbf{i}_K^\perp(\theta_K) \equiv -\sin(\theta_K) \mathbf{i}_x + \cos(\theta_K) \mathbf{i}_y \quad (154)$$

specified by that analyzer's HWP orientation. Using these data, we are to evaluate the CHSH S parameter

$$S \equiv \left| E\left(0, \frac{3\pi}{8}\right) + E\left(\frac{-\pi}{4}, \frac{3\pi}{8}\right) + E\left(\frac{-\pi}{4}, \frac{\pi}{8}\right) - E\left(0, \frac{\pi}{8}\right) \right| \quad (155)$$

where

$$E(\theta_A, \theta_B) \equiv \langle a(\theta_A) b(\theta_B) \rangle \quad (156)$$

with $a(\theta_A) = 1$ if $\mathbf{i}_A(\theta_A)$ is detected, $a(\theta_A) = -1$ if $\mathbf{i}_A^\perp(\theta_A)$ is detected, and likewise for $b(\theta_B)$.

According to local hidden variables theory, there is an underlying classical random variable v associated with the photon pair such that each analyzer's measurement outcome is a deterministic function of v and its HWP setting. We then have that

$$S = \left| \int dv \left\{ \left[a(0, v) + a\left(\frac{-\pi}{4}, v\right) \right] b\left(\frac{3\pi}{8}, v\right) + \left[a\left(\frac{-\pi}{4}, v\right) - a(0, v) \right] b\left(\frac{\pi}{8}, v\right) \right\} p(v) \right| \quad (157)$$

where $p(v)$ is the hidden variable's probability density function. Because $a(\theta_A, v) = \pm 1$, we have that both $\mathcal{B}_+(v) \equiv a(0, v) +$

⁵As yet, of course, no loophole-free violation of the CHSH inequality has been demonstrated, but that has not detracted from its use as a metric for sources of polarization-entangled photons.

$a(-\pi/4, v)$ and $\mathcal{B}_-(v) \equiv a(-\pi/4, v) - a(0, v)$ must equal either -2 , 0 , or $+2$. Moreover, if the former equals ± 2 , then the latter must equal zero, and *vice versa*. Thus, we can separate the integral in (157) into integrals over two nonoverlapping regions: \mathcal{M}_+ , wherein \mathcal{B}_+ is nonzero, and \mathcal{M}_- , wherein \mathcal{B}_- is nonzero. Deriving the CHSH inequality is now straightforward. For any hidden variables theory, we have

$$S = \left| \int_{\mathcal{M}_+} dv \mathcal{B}_+(v) b\left(\frac{3\pi}{8}, v\right) p(v) + \int_{\mathcal{M}_-} dv \mathcal{B}_-(v) b\left(\frac{\pi}{8}, v\right) p(v) \right| \quad (158)$$

$$\leq \int_{\mathcal{M}_+} dv |\mathcal{B}_+(v) b\left(\frac{3\pi}{8}, v\right)| p(v) + \int_{\mathcal{M}_-} dv |\mathcal{B}_-(v) b\left(\frac{\pi}{8}, v\right)| p(v) \quad (159)$$

$$= \int_{\mathcal{M}_+} dv 2p(v) + \int_{\mathcal{M}_-} dv 2p(v) = 2 \quad (160)$$

where the penultimate inequality follows from $|\mathcal{B}_\pm(v) b(\theta_B, v)| = 2$.

The polarization singlet state

$$|\psi^-\rangle_{AB} \equiv \frac{|x\rangle_A |y\rangle_B - |y\rangle_A |x\rangle_B}{\sqrt{2}} \quad (161)$$

where $|k\rangle_K$ denotes a single photon polarized along $k = x$ or y for light directed to polarization analyzer $K = A$ or B , violates the $S \leq 2$ limit of hidden variables theory. It is easily shown that this state leads to

$$E(\theta_A, \theta_B) = -\cos[2(\theta_A - \theta_B)] \quad (162)$$

whence $S = 2\sqrt{2}$, by substituting into (155). Experiments that yield S parameters greater than 2 cannot be explained by means of hidden variables, i.e., they violate locality. Experiments that seek to demonstrate such a CHSH violation using the light produced by SPDC face several issues that were omitted from our simple polarization singlet calculation. At a fundamental level, there are loopholes through which hidden variables may permit $S > 2$, e.g., when the detectors have subunity quantum efficiencies [60], or when the HWP settings at each analysis station are not space-like separated [61]. At a more mundane level, a pair of coherently pumped CW downconverters only produces a statistically stationary, zero-mean, jointly Gaussian state of signal and idler beams that, after postselection, *approximates* the frequency-entangled polarization singlet state from (139) when the detection interval is sufficiently short. To conclude this section, we apply quantum photodetection theory and Gaussian-state analysis to quantify the CHSH violation obtained from SPDC experiments.

The setup for testing the CHSH inequality with SPDC light is shown in Fig. 10. Here, two frequency-degenerate, type-II phase-matched, CW downconverters are pumped π rad out-of-phase, and their outputs combined, as in [57], with a 90° polarization rotation. Fiber coupling is employed to select single spatial modes of the resulting signal and idler beams. The excited

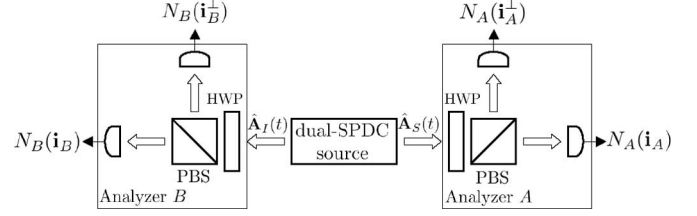


Fig. 10. Setup for testing the CHSH inequality with a dual-SPDC source.

spatial modes can then be taken to be $\hat{\mathbf{A}}_S(t)e^{-j\omega_P t/2}/\sqrt{A_d}$, and $\hat{\mathbf{A}}_I(t)e^{-j\omega_P t/2}/\sqrt{A_d}$ for $\rho \in \mathcal{A}_d$, where $\hat{\mathbf{A}}_S(t)$ and $\hat{\mathbf{A}}_I(t)$ are baseband vector field operators that represent the x and y polarization components of the signal and idler.⁶ With this source arrangement, the baseband field operators are in a statistically stationary, zero-mean, jointly Gaussian state whose nonzero covariances are

$$K_{A_{K_k} A_{K_k}}^{(n)}(\tau) = K^{(n)}(\tau), \quad \text{for } K = S, I, k = x, y \quad (163)$$

$$K_{A_{S_x} A_{I_y}}^{(p)}(\tau) = -K_{A_{S_y} A_{I_x}}^{(p)}(\tau) = K_{A_S A_I}^{(p)}(\tau) \quad (164)$$

where $K^{(n)}(\tau)$ and $K_{A_S A_I}^{(p)}(\tau)$ are as given in (141) and (142), respectively. All the detectors in Fig. 10 have quantum efficiency η and collect photon counts whose measurement statistics are equivalent to those of the observables

$$\hat{N}_K(\mathbf{i}_K) \equiv \int_0^{T_c} dt [\mathbf{i}_K \cdot \hat{\mathbf{A}}'_K(t)]^\dagger [\mathbf{i}_K \cdot \hat{\mathbf{A}}'_K(t)] \quad (165)$$

$$\hat{N}_K(\mathbf{i}_K^\perp) \equiv \int_0^{T_c} dt [\mathbf{i}_K^\perp \cdot \hat{\mathbf{A}}'_K(t)]^\dagger [\mathbf{i}_K^\perp \cdot \hat{\mathbf{A}}'_K(t)] \quad (166)$$

for $K = A, B$, where $\hat{\mathbf{A}}'_K(t) = \sqrt{\eta} \hat{\mathbf{A}}_K(t) + \sqrt{1-\eta} \hat{\mathbf{A}}_{K_\eta}(t)$ is our usual vacuum-state quantum noise injection to account for $\eta < 1$ photodetection. Paralleling our development of photon-coincidence counting in HOM interferometry, we can evaluate the average number of coincidence counts $C(\theta, \theta') \equiv \langle N_A(\mathbf{i}(\theta)) N_B(\mathbf{i}(\theta')) \rangle$ for arbitrary HWP settings. We find that

$$C(\theta_A, \theta_B) = \left(\frac{\eta P T_c}{\hbar \omega_P / 2} \right)^2 + \frac{\eta^2 P T_c}{\hbar \omega_P / 2} \sin^2(\theta_A - \theta_B) \quad (167)$$

$$C(\theta_A, \theta_B^\perp) = \left(\frac{\eta P T_c}{\hbar \omega_P / 2} \right)^2 + \frac{\eta^2 P T_c}{\hbar \omega_P / 2} \cos^2(\theta_A - \theta_B) \quad (168)$$

$$C(\theta_A^\perp, \theta_B) = \left(\frac{\eta P T_c}{\hbar \omega_P / 2} \right)^2 + \frac{\eta^2 P T_c}{\hbar \omega_P / 2} \cos^2(\theta_A - \theta_B) \quad (169)$$

$$C(\theta_A^\perp, \theta_B^\perp) = \left(\frac{\eta P T_c}{\hbar \omega_P / 2} \right)^2 + \frac{\eta^2 P T_c}{\hbar \omega_P / 2} \sin^2(\theta_A - \theta_B) \quad (170)$$

where the first term in each of these expressions is the number of accidental coincidences. Under typical operating conditions, this number will be much smaller than $2\eta^2 P T_c / \hbar \omega_P$.

⁶For the CHSH violation, it is not necessary that the downconverters be operated at frequency degeneracy. We have chosen to do so for notational convenience.

Because the probability of the SPDC source producing a photon pair in the interval $0 \leq t \leq T_c$ is quite small, we obtain the $E(\theta_A, \theta_B)$ values needed for evaluating the CHSH S parameter from the fair-sampling formula [12]

$$E(\theta_A, \theta_B) = \frac{C(\theta_A, \theta_B) + C(\theta_A^\perp, \theta_B^\perp) - C(\theta_A^\perp, \theta_B) - C(\theta_A, \theta_B^\perp)}{C(\theta_A, \theta_B) + C(\theta_A^\perp, \theta_B^\perp) + C(\theta_A^\perp, \theta_B) + C(\theta_A, \theta_B^\perp)} \quad (171)$$

$$= \frac{1 - (\hbar\omega_P/4PT_c) \cos[2(\theta_A - \theta_B)]}{1 + \hbar\omega_P/4PT_c}. \quad (172)$$

With this result, we obtain the following value for the S parameter:

$$S = \frac{2 + 2\sqrt{2} \hbar\omega_P/4PT_c}{1 + \hbar\omega_P/4PT_c} \approx 2\sqrt{2} \quad (173)$$

where approximation employs $PT_c/\hbar\omega_P \ll 1$, i.e., the probability of the source emitting a photon pair within a coincidence interval is very small. For reasonable values of η , this condition is the same as saying that the accidental coincidences can be neglected.

V. CLASSICAL INFORMATION CAPACITIES OF BOSONIC CHANNELS

Information theory seeks to delineate the ultimate limits on reliable communication that arise from the presence of noise and other disturbances, and to establish means by which these limits can be approached in practical systems. The mathematical foundation for this assessment of limits is Shannon's noisy channel coding theorem [62], [63], which introduced the notion of channel capacity—the maximum mutual information between a channel's input and output—as the highest rate at which error-free communication could be maintained. Textbook treatments of channel capacity [35], [64] study channel models—ranging from the binary symmetric channel's digital abstraction to the additive white Gaussian noise channel's idealization of thermal-noise-limited waveform transmission—for which classical physics is the underlying paradigm. Despite the success of Shannon theory for classical information transmission, it does not respect the underlying quantum nature of electromagnetic fields. In particular, when it is applied to optical communication systems—for which quantum noise sets the fundamental performance limits—the standard presumptions are that the transmitters employ classical-state light, and the receivers use direct, homodyne, or heterodyne detection, so that semiclassical theory (shot-noise plus excess-noise analysis) suffices. Imposing these structural assumptions on optical communication transmitters and receivers, however, precludes optimization over the use of nonclassical states at the transmitter, and nonstandard quantum measurements at the receiver. Thus, to derive the true classical information capacities of optical channels, we need a version of Shannon theory that is unfettered by such restrictions on the transmission system, viz., the Holevo–Schumacher–Westmoreland (HSW) theorem [65]–[67]. In this, our final section, we shall review application of the HSW theorem to bosonic

(optical communication) channels, concentrating on single-user transmission over a line-of-sight free-space path. It is convenient to begin with the single-mode treatment.

A. Single-Mode Channel Models and Capacity Results

We are interested in the classical communication capacities of three bosonic channels with isotropic Gaussian noise—the lossy channel, the amplifying channel, and the classical-noise channel—whose single-mode propagation characteristics are as follows. In each case, the channel input is an electromagnetic field mode with annihilation operator \hat{a} , and the channel output is another field mode with annihilation operator \hat{a}' . None of these channels constitute unitary evolutions; therefore, they are all governed by trace-preserving completely positive (TPCP) maps [68] that relate their output density operators $\hat{\rho}'$ to their input density operators $\hat{\rho}$.

The TPCP map $\mathcal{E}_\eta^N(\cdot)$ for the single-mode lossy channel can be derived from the commutator-preserving beam splitter relation

$$\hat{a}' = \sqrt{\eta} \hat{a} + \sqrt{1-\eta} \hat{b} \quad (174)$$

in which the annihilation operator \hat{b} is associated with an environmental (noise) mode, and $0 \leq \eta \leq 1$ is the channel transmissivity. For the pure-loss channel, the \hat{b} mode is in its vacuum state; for the thermal-noise channel, this mode is in a thermal state, viz., an isotropic Gaussian mixture of coherent states with average photon number $N > 0$

$$\hat{\rho}_b = \int d^2\alpha \frac{\exp(-|\alpha|^2/N)}{\pi N} |\alpha\rangle\langle\alpha|. \quad (175)$$

The TPCP map $\mathcal{A}_\kappa^N(\cdot)$ for the single-mode amplifying channel can be derived from the commutator-preserving phase-insensitive amplifier relation

$$\hat{a}' = \sqrt{\kappa} \hat{a} + \sqrt{\kappa-1} \hat{c}^\dagger \quad (176)$$

where \hat{c} is the modal annihilation operator for the noise introduced by the amplifier and $\kappa \geq 1$ is the amplifier gain. This amplifier injects the minimum possible noise when the \hat{c} -mode is in its vacuum state. We will also be concerned with the excess-noise case, in which the \hat{c} mode's density operator is the isotropic Gaussian coherent-state mixture

$$\hat{\rho}_c = \int d^2\alpha \frac{\exp(-|\alpha|^2/N)}{\pi N} |\alpha\rangle\langle\alpha| \quad (177)$$

with average photon number $N > 0$.

The classical-noise channel can be viewed as the cascade of a pure-loss channel \mathcal{E}_η^0 followed by a minimum-noise amplifying channel \mathcal{A}_κ^0 whose gain exactly compensates for the loss $\kappa = 1/\eta$. Then, with $\eta = 1/(M+1)$, we obtain the following TPCP map for the classical-noise channel

$$\hat{\rho}' = \mathcal{N}_M(\hat{\rho}) \equiv \int d^2\alpha \frac{\exp(-|\alpha|^2/M)}{\pi M} \hat{D}(\alpha) \hat{\rho} \hat{D}^\dagger(\alpha) \quad (178)$$

where $\hat{D}(\alpha)$ is the displacement operator that maps the coherent state $|\alpha_0\rangle$ into the coherent state $|\alpha_0 + \alpha\rangle$. This TPCP map is equivalent to the annihilation operator input–output relation

$\hat{a}' = \hat{a} + m$, where m is a zero-mean, isotropic, complex-valued Gaussian noise with variance given by $\langle |m|^2 \rangle = M$, thus making it the quantum version of the additive white Gaussian noise channel whose capacity was defined and derived by Shannon.

The classical capacity of a quantum channel is established by random coding arguments akin to those employed in classical information theory. A set of symbols $\{j\}$ is represented by a collection of input states (density operators) $\{\hat{\rho}_j\}$ that are selected according to some prior distribution $\{p_j\}$. The output states $\{\hat{\rho}'_j\}$ are obtained by applying the channel's TPCP map $\mathcal{E}(\cdot)$ to these input symbols. The Holevo information associated with priors $\{p_j\}$ and states $\{\hat{\sigma}_j\}$ is given by

$$\chi(p_j, \hat{\sigma}_j) = S\left(\sum_j p_j \hat{\sigma}_j\right) - \sum_j p_j S(\hat{\sigma}_j) \quad (179)$$

where $S(\hat{\sigma}) \equiv -\text{tr}(\hat{\sigma} \ln(\hat{\sigma}))$ is the von Neumann entropy. According to the HSW theorem, the capacity of this channel, in nats per use, is

$$C = \sup_n \left(\frac{C_n}{n} \right) = \sup_n \left\{ \max_{\{p_j, \hat{\rho}_j\}} \left[\frac{\chi(p_j, \mathcal{E}^{\otimes n}(\hat{\rho}_j))}{n} \right] \right\} \quad (180)$$

where C_n is the capacity achieved when coding is performed over n -channel-use symbols, and the supremum over n is necessitated by the fact that channel capacity may be superadditive.

The lossless channel is governed by the TPCP map $\mathcal{E}_1^0(\cdot) = \mathcal{A}_1^0(\cdot)$. It has long been known [32], [69] that the capacity of the single-mode lossless channel—subject to a constraint N_S on the transmitter's average photon number—is additive. It is achieved by random single-channel-use coding over number states using a Bose–Einstein prior, which yields

$$C = g(N_S) \equiv (N_S + 1) \ln(N_S + 1) - N_S \ln(N_S) \quad (181)$$

for the capacity in nats per use. Note that because the channel is lossless, transmission of the number state $|n\rangle$ implies reception of the same number state. Thus, the probability of confusing distinct codewords is zero. Moreover, because the von Neumann entropy of a pure state is zero, we have that the preceding C expression represents the maximum von Neumann entropy of a single-mode field state whose average photon number is at most N_S . Note that this capacity-achieving system, for the lossless channel, uses nonclassical (number state) light, but a conventional (photon counting) receiver.

More than a decade after the capacity proof for the lossless bosonic channel, we derived the capacity for the pure-loss channel [18]. Under the same average photon number constraint at the transmitter, we found that the pure-loss channel's capacity is additive and given by

$$C = g(\eta N_S), \quad \text{for } 0 \leq \eta \leq 1 \quad (182)$$

in nats per use, where capacity is achieved by random-coding over coherent states using the isotropic Gaussian probability density function

$$p(\alpha) = \frac{e^{-|\alpha|^2/N_S}}{\pi N_S}. \quad (183)$$

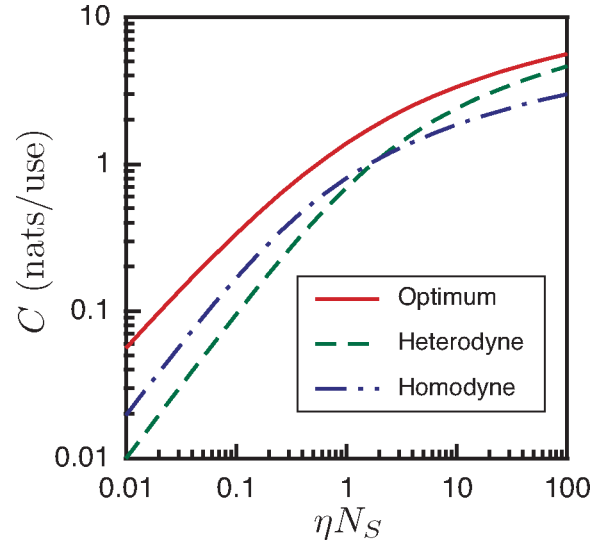


Fig. 11. Comparison of channel capacities, in nats per channel use, for the pure-loss channel. The solid curve is the optimum capacity from the HSW theorem. The dashed curve is the capacity for coherent-state encoding with heterodyne detection. The dot-dashed curve is the capacity for coherent-state encoding with homodyne detection.

Because our demonstration included the lossless $\eta = 1$ case, it showed that the capacity in (181) could also be achieved with coherent states, i.e., classical-state light. With classical-state encoding, however, the conventional reception techniques do *not* achieve capacity. Indeed, as of today, no explicit realization is known for a receiver that can realize the random coding capacity given by (182). The extent to which this ultimate capacity exceeds what can be achieved with conventional systems will, therefore, provide the impetus for seeking that receiver realization. Fig. 11 illustrates the capacity advantage afforded by the HSW theorem for the pure-loss channel by comparing the quantum result from (182) with the capacities achieved over this bosonic channel when optical homodyne or heterodyne detection is employed in conjunction with coherent-state encoding, namely⁷

$$C_{\text{hom}} = \frac{\ln(1 + 4\eta N_S)}{2} \quad (184)$$

and

$$C_{\text{het}} = \ln(1 + \eta N_S). \quad (185)$$

The crossing of the heterodyne and homodyne capacity-versus-photon-number curves in Fig. 11 occurs because heterodyne detection has twice the bandwidth of homodyne detection, but twice the noise level in each quadrature. Consequently, the former outperforms the latter at high N_S values with the converse being true at low N_S values. Note that squeezed states can be used, with homodyne detection, to achieve a higher capacity than the coherent-state homodyne capacity from (184) when the channel is lossless, i.e., when $\eta = 1$ [32]. This advantage

⁷As we have seen, in Section IV, homodyne and heterodyne detection of coherent-state light yields a Gaussian noise channel. Hence, these capacities (in nats per use) are easily found from standard Shannon theory formulas.

quickly reduces to an inconsequential amount when $\eta \ll 1$, which is the typical propagation situation for both free-space and fiber channels.

The direct-detection capacity (in nats per use) for this single-mode case is not known, but has been shown to obey [70], [71]

$$C_{\text{dir}} \leq \frac{1}{2} \ln(\eta N_S) + o(1) \quad (186)$$

and

$$\lim_{N_S \rightarrow \infty} C_{\text{dir}} = \frac{1}{2} \ln(\eta N_S). \quad (187)$$

Therefore, C_{dir} is dominated by (182) for $\ln(\eta \bar{N}) > 1$, although it has been shown [72] that

$$\lim_{N_S \rightarrow 0} C_{\text{dir}} = C \quad (188)$$

so that direct detection is asymptotically optimal in this regime. At high N_S values, it turns out that heterodyne detection is asymptotically optimal [33], viz.,

$$\lim_{N_S \rightarrow \infty} \frac{C_{\text{het}}}{C} = 1. \quad (189)$$

In subsequent work [33], we addressed the capacity of the thermal-noise channel. There, we showed that the rate achieved with single-letter, coherent-state encoding using the same probability density that achieved capacity for the pure-loss channel is given (in nats per use) by

$$R = g(\eta N_S + (1 - \eta)N) - g[(1 - \eta)N] \quad (190)$$

and is a lower bound on C . We also conjectured that this lower bound is, in fact, the capacity. Our capacity conjecture is intimately related to our work [26] on the minimum output entropy for the thermal-noise channel. Indeed, the following minimum output entropy conjecture suffices to prove that $C = R$ for the thermal-noise channel.

Conjecture—Let the environmental modes $\hat{\mathbf{b}} = (\hat{b}_1, \hat{b}_2, \dots, \hat{b}_n)$ be in a tensor product of n thermal states with total von Neumann entropy $ng(K)$. Then, the von Neumann entropy of the output modes $\hat{\mathbf{a}}' = (\hat{a}'_1, \hat{a}'_2, \dots, \hat{a}'_n) = \sqrt{\eta} \hat{\mathbf{a}} + \sqrt{1 - \eta} \hat{\mathbf{b}}$ is minimized when the input modes $\hat{\mathbf{a}} = (\hat{a}_1, \hat{a}_2, \dots, \hat{a}_n)$ are in their vacuum states. The resulting minimum von Neumann output entropy is $ng[(1 - \eta)K]$.

The output entropy from a bosonic channel, such as the thermal-noise channel, when one of its inputs is in a pure state is a measure of the degree to which the channel output is entangled with its environment. Therefore, it seems eminently reasonable that the input state that will result in the least entanglement with the environment is the vacuum state.⁸ Nevertheless, despite considerable effort, neither the conjecture nor its weak ($n = 1$) form has been proven. It is known, for example, that the conjecture is true in the limits of low and high noise, and it is known that the vacuum-state input yields a local minimum of the output entropy. For other evidence supportive of this conjecture, see [26].

⁸The output entropy is invariant to the input state's mean field; therefore, any coherent state will give the same output entropy as the vacuum state, i.e., uniqueness is not a necessary ingredient in the preceding conjecture.

The situation with respect to the capacities of the amplifying and the classical-noise channels is similar to what we have just stated for the thermal-noise channel. Coherent-state encoding with an isotropic Gaussian prior yields achievable rates [33] in nats per channel use

$$R = g[\kappa N_S + (\kappa - 1)(N + 1)] - g[(\kappa - 1)(N + 1)] \quad (191)$$

for the amplifying channel, and

$$R = g(N_S + M) - g(M) \quad (192)$$

for the classical-noise channel, thus providing lower bounds on the capacities of these channels. Moreover, these rates exceed the capacities achievable with the conventional optical reception techniques.⁹ Proving the minimum output entropy conjecture would establish that (192) is, in fact, the classical-noise channel's capacity. Proving a similar conjecture for the amplifying channel would show that (191) is that channel's capacity.

B. Capacity of the Far-Field Free-Space Channel

Our culminating material on the quantum theory of optical communications unites quantum diffraction theory—and its modal decomposition—with the HSW theorem to determine the classical information capacity of the line-of-sight free-space channel. We shall assume the propagation geometry shown in Fig. 1, wherein the transmitter controls the state of the \mathcal{A}_0 -pupil input field operator $\hat{E}_0(\boldsymbol{\rho}, t)$, the receiver has access only to the \mathcal{A}_L -pupil output field operator $\hat{E}_L(\boldsymbol{\rho}, t)$, and $\mathcal{D}_F = A_0 A_L / (\lambda_0 L)^2 \ll 1$, so that we are in the far-field power-transfer regime. We shall restrict our transmitter to using the maximum power-transfer input spatial mode, whose power-transfer eigenvalue is $\eta_1 \approx D_f$. Moreover, the transmitter will also be constrained such that it only excites frequencies within a quasi-monochromatic band $\pm \Omega_0$ around ω_0 , and is limited to an average power P_S . The environmental (background) noise entering this receiver in each spatiotemporal mode within the frequency band of interest is an independent, isotropic mixture of coherent states with average photon number [73]

$$N = \frac{\pi 10^6 \lambda_0^3 N_\lambda}{\hbar \omega_0^2} \quad (193)$$

where N_λ is the background spectral radiance (in $\text{W/m}^2 \text{sr } \mu\text{m}$). A typical daytime value ($N_\lambda \sim 10 \text{ W/m}^2 \text{sr } \mu\text{m}$) at $\lambda_0 = 1.55 \mu\text{m}$ then leads to $N \sim 10^{-6}$; nighttime N_λ values are several orders of magnitude lower [73].¹⁰

Because the single-mode, thermal-noise channel $\mathcal{E}_{\eta_1}^N$ is the concatenation of the pure-loss channel $\mathcal{E}_{\eta_1}^0$ with a classical-noise channel of average noise-photon number $(1 - \eta)N$ [26], it follows that the capacity of a thermal-noise channel can never

⁹Again, we see that classical-state encoding with nonstandard measurements outperforms the same encoding with conventional photodetection receivers.

¹⁰Here, we are including the background noise that would be encountered in a line-of-sight terrestrial link, treating the rest of the propagation as though it were in free space. A more complete development—for clear-weather operation—would include both atmospheric extinction and atmospheric turbulence effects. The former is easily incorporated into HSW theorem analysis [74], but no such development has been made for the latter.

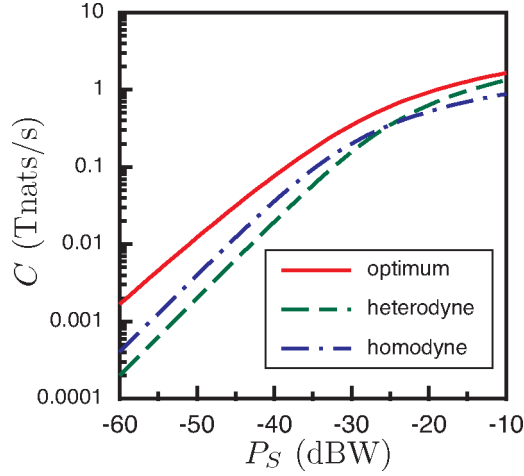


Fig. 12. Capacities versus transmitter power for the single spatial-mode, quasi-monochromatic, 1.55- μm -wavelength channel for optimum reception (solid curve), heterodyne detection (dashed curve), and homodyne detection (dot-dashed curve). These capacities assume that $\Omega_0/2\pi = 1$ THz, $d_0 = 1$ mm, $d_L = 1$ cm, and $L = 1$ km.

exceed that of the pure-loss channel with the same transmissivity. As a result, the optimal-reception capacity of a single temporal mode of our single spatial-mode channel satisfies

$$g[\eta_1 N_S + (1 - \eta_1)N_S] - g[(1 - \eta_1)N] \leq C \leq g(\eta_1 N_S) \quad (194)$$

and these single-mode-capacity upper and lower bounds are virtually coincident for $\eta_1 N_S \geq 10(1 - \eta_1)N$. For the quasi-monochromatic, multiple temporal-mode, single spatial-mode case, we then have the following bounds [74] on the channel capacity in nats per second:

$$\begin{aligned} \frac{\Omega_0}{\pi} \left\{ g \left[\frac{\eta_1 \pi P_S}{\hbar \omega_0 \Omega_0} + (1 - \eta_1)N \right] - g[(1 - \eta_1)N] \right\} \\ \leq C \leq \frac{\Omega_0}{\pi} g \left(\frac{\eta_1 \pi P_S}{\hbar \omega_0 \Omega_0} \right). \end{aligned} \quad (195)$$

So long as $\eta_1 \pi P_S / \hbar \omega_0 \Omega_0 \geq 10(1 - \eta_1)N$, these bounds are exceedingly tight, and background light can be neglected in determining the capacity achieved with optimum reception. The impact of the background light on the multiple temporal-mode channel capacities of homodyne and heterodyne detection is also negligible, because these capacities are given by

$$C_{\text{hom}} = \frac{\Omega_0}{2\pi} \ln \left(1 + \frac{\eta_1 4\pi P_S / \hbar \omega_0 \Omega_0}{1 + 2(1 - \eta_1)N} \right) \quad (196)$$

$$C_{\text{het}} = \frac{\Omega_0}{\pi} \ln \left(1 + \frac{\eta_a \pi P_S / \hbar \omega_0 \Omega_0}{1 + (1 - \eta_1)N} \right) \quad (197)$$

and we have $N \ll 1$.

In Figs. 12 and 13, we have plotted the single-spatial-mode, quasi-monochromatic, 1.55- μm -wavelength capacities versus power (Fig. 12) and path length (Fig. 13). Both of these plots assume that $\Omega_0/2\pi = 1$ THz, $A_0 = \pi d_0^2/4$ with $d_0 = 1$ mm, and $A_L = \pi d_L^2/4$ with $d_L = 1$ cm. Fig. 12 assumes that $L = 1$ km, and Fig. 13 assumes that $P_S = 1$ mW. These numbers represent a ~ 1 mR transmitter-beam divergence, and transmitter powers

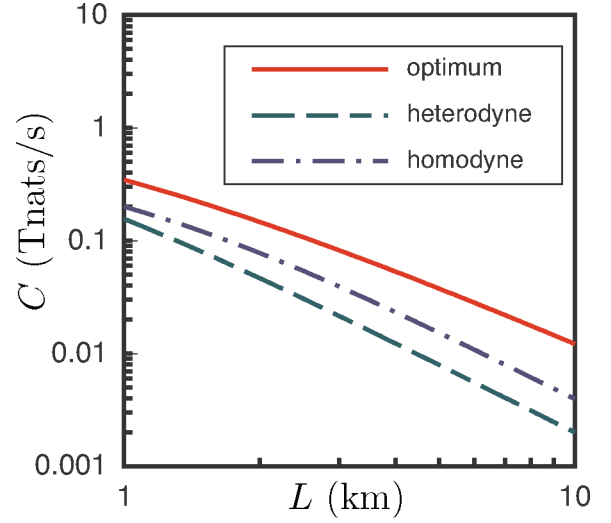


Fig. 13. Capacities versus path length for the single spatial-mode, quasi-monochromatic, 1.55- μm -wavelength channel for optimum reception (solid curve), heterodyne detection (dashed curve), and homodyne detection (dot-dashed curve). These capacities assume that $\Omega_0/2\pi = 1$ THz, $d_0 = 1$ mm, $d_L = 1$ cm, and $P_S = 1$ mW.

commensurate with semiconductor-laser/power-amplifier technology. The curves show that optimum reception increasingly outstrips homodyne and heterodyne detection at lower transmitter powers and longer path lengths. At high enough power levels in the far field—or if operation is in the near-field regime—capacity can be increased substantially beyond what we have presented by employing multiple spatial modes [74], [75].

VI. CONCLUSION

In this paper, we have reviewed the underpinnings of the quantum theory of optical communications, with emphasis on free-space propagation, and the distinction between the semiclassical and quantum theories of photodetection. Even in a paper of this length, we could not do complete justice to these topics, much less to many other relevant applications. One area of current interest, for which the machinery developed herein is of direct use, is the study of quantum imaging, cf., the biphoton treatment of ghost imaging [29] with the full Gaussian-state analysis of such a system [76]. The latter has been especially helpful in comparing ghost imaging done with classical-state light versus that done with SPDC light, and in computing the image SNRs that are achieved with these two sources [77]. Another topic that was omitted is the limits on the transmission of *quantum* information over bosonic channels [78], [79]. Within the realm of classical information transmission, results are available for multiuser configurations, i.e., multiple-access (analogous to the cell phone uplink) [80] and broadcast (analogous to the cell phone downlink) [81]. Doubtless the reader will find many other areas in which nonclassical light and/or quantum photodetection will be of use in providing performance capabilities that—at least in principle—outstrip what is possible with classical-state transmitters and conventional photodetection receivers. Such demonstrations will then continue to spur the development of the nonclassical light sources and the

optimum or near-optimum measurement systems required to reap the predicted performance benefits.

Note Added in Proof: Subsequent to the acceptance of this paper the two minimum output entropy conjectures mentioned in Section V-A have been proven [82], [83]. Thus is it now known that the thermal-noise, amplifying, and classical-noise bosonic channels are additive, with single-mode capacities given by (190)–(192), respectively. Likewise, the lower bound in (195) is the capacity for the far-field free-space channel from Section V-B.

ACKNOWLEDGMENT

The author's work on the quantum theory of optical communications has benefited from collaborations with many colleagues and students over the past 30 years. There are too many names to list here, but it would be remiss not to acknowledge Prof. H. Yuen of Northwestern University, with whom the author began the research journey that ultimately led to this paper.

REFERENCES

- [1] V. W. S. Chan, "Optical satellite networks," *J. Lightw. Technol.*, vol. 21, no. 11, pp. 2811–2827, Nov. 2003.
- [2] V. W. S. Chan, "Optical space communications," *IEEE J. Sel. Topics Quantum Electron.*, vol. 6, no. 6, pp. 959–975, Nov./Dec. 2000.
- [3] V. W. S. Chan, "Free-space optical communications," *J. Lightw. Technol.*, vol. 24, no. 12, pp. 4750–4762, Dec. 2006.
- [4] D. J. T. Healey, D. R. Wisely, I. Neild, and P. Cochrane, "Optical wireless: The story so far," *IEEE Commun. Mag.*, vol. 36, no. 12, pp. 72–74, pp. 79–82, Dec. 1998.
- [5] D. Kedar and S. Arnon, "Urban optical wireless communication networks: The main challenges and possible solutions," *IEEE Commun. Mag.*, vol. 42, no. 5, pp. S2–S7, May 2004.
- [6] R. M. Gagliardi and S. Karp, *Optical Communications*. New York: Wiley, 1976.
- [7] J. Goward, *Optical Communication Systems*. Englewood Cliffs, NJ: Prentice-Hall, 1984.
- [8] H. P. Yuen and J. H. Shapiro, "Optical communication with two-photon coherent states—Part III: Quantum measurements realizable with photoemissive detectors," *IEEE Trans. Inf. Theory*, vol. 26, no. 1, pp. 78–92, Jan. 1980.
- [9] V. Zwiller, H. Blom, P. Jonsson, N. Panev, S. Jeppesen, T. Tsegaye, and E. Goobar, "Single quantum dots emit single photons at a time: Antibunching experiments," *Appl. Phys. Lett.*, vol. 78, no. 17, pp. 2476–2478, Apr. 2001.
- [10] R. E. Slusher, L. W. Hollberg, B. Yurke, J. C. Mertz, and J. F. Valley, "Observation of squeezed states generated by four-wave mixing in an optical cavity," *Phys. Rev. Lett.*, vol. 55, no. 22, pp. 2409–2412, Nov. 1985.
- [11] Z. Y. Ou and L. Mandel, "Violation of Bell's inequality and classical probability in a two-photon correlation experiment," *Phys. Rev. Lett.*, vol. 61, no. 1, pp. 50–53, Jul. 1988.
- [12] P. G. Kwiat, K. Mattle, H. Weinfurter, A. Zeilinger, A. V. Sergienko, and Y. Shih, "New high-intensity source of polarization-entangled photon pairs," *Phys. Rev. Lett.*, vol. 75, no. 24, pp. 4337–4341, Dec. 1995.
- [13] E. Knill, R. Laflamme, and G. J. Milburn, "A scheme for efficient quantum computation with linear optics," *Nature (London)*, vol. 409, no. 6816, pp. 46–52, Jan. 2001.
- [14] S. L. Braunstein and P. van Loock, "Quantum information with continuous variables," *Rev. Mod. Phys.*, vol. 77, no. 2, pp. 513–577, Apr. 2005.
- [15] D. Bouwmeester, J.-W. Pan, K. Mattle, M. Eibl, H. Weinfurter, and A. Zeilinger, "Experimental quantum teleportation," *Nature (London)*, vol. 390, no. 6660, pp. 575–579, Dec. 1997.
- [16] A. Furusawa, J. L. Sørensen, S. L. Braunstein, C. A. Fuchs, H. J. Kimble, and E. S. Polzik, "Unconditional quantum teleportation," *Science*, vol. 282, no. 5389, pp. 706–709, Oct. 1998.
- [17] J. H. Shapiro, "Single-photon Kerr nonlinearities do not help quantum computation," *Phys. Rev. A*, vol. 73, no. 6, pp. 062305-1–062305-11, Jun. 2006.
- [18] V. Giovannetti, S. Guha, S. Lloyd, L. Maccone, J. H. Shapiro, and H. P. Yuen, "Classical capacity of lossy bosonic channels: The exact solution," *Phys. Rev. Lett.*, vol. 92, no. 2, pp. 027902-1–027902-4, Jan. 2004.
- [19] W. H. Louisell, *Quantum Statistical Properties of Radiation*. New York: Wiley, 1973, ch. 4.
- [20] H. P. Yuen and J. H. Shapiro, "Optical communication with two-photon coherent states—Part I: Quantum state propagation and quantum noise reduction," *IEEE Trans. Inf. Theory*, vol. IT-24, no. 6, pp. 657–668, Nov. 1978.
- [21] D. Slepian, "Analytic solution of two apodization problems," *J. Opt. Soc. Amer.*, vol. 55, no. 9, pp. 1110–1115, Sep. 1965.
- [22] J. H. Shapiro, "Quantum Gaussian noise," *Proc. SPIE*, vol. 5111, pp. 382–395, 2003.
- [23] R. J. Glauber, "Optical coherence and photon statistics," in *Quantum Optics and Electronics*, C. DeWitt, A. Blandin, and C. Cohen-Tannoudji, Eds. New York: Gordon and Breach, 1965.
- [24] R. S. Bondurant and J. H. Shapiro, "Squeezed states in phase-sensing interferometers," *Phys. Rev. D*, vol. 30, no. 12, pp. 2548–2556, Dec. 1984.
- [25] M. Xiao, L.-A. Wu, and H. J. Kimble, "Precision measurement beyond the shot-noise limit," *Phys. Rev. Lett.*, vol. 59, no. 3, pp. 278–281, Jul. 1987.
- [26] V. Giovannetti, S. Guha, S. Lloyd, L. Maccone, and J. H. Shapiro, "Minimum output entropy of bosonic channels: A conjecture," *Phys. Rev. A*, vol. 70, no. 3, pp. 032315-1–032315-14, Sep. 2004.
- [27] F. N. C. Wong, J. H. Shapiro, and T. Kim, "Efficient generation of polarization-entangled photons in a nonlinear crystal," *Laser Phys.*, vol. 16, no. 11, pp. 1517–1524, Nov. 2006.
- [28] C. K. Hong and L. Mandel, "Experimental realization of a localized one-photon state," *Phys. Rev. Lett.*, vol. 56, no. 1, pp. 56–58, Jan. 1986.
- [29] T. B. Pittman, B. C. Jacobs, and J. D. Franson, "Heralding single photons from pulsed parametric down-conversion," *Opt. Commun.*, vol. 246, no. 4–6, pp. 545–550, Feb. 2005.
- [30] C. K. Hong, Z. Y. Ou, and L. Mandel, "Measurement of subpicosecond time intervals between two photons by interference," *Phys. Rev. Lett.*, vol. 59, no. 18, pp. 2044–2046, Nov. 1987.
- [31] J. F. Clauser, M. A. Horne, A. Shimony, and R. A. Holt, "Proposed experiment to test local hidden variable theories," *Phys. Rev. Lett.*, vol. 23, no. 15, pp. 880–884, Oct. 1969.
- [32] C. M. Caves and P. D. Drummond, "Quantum limits on bosonic communication rates," *Rev. Mod. Phys.*, vol. 66, no. 2, pp. 481–537, Apr. 1994.
- [33] J. H. Shapiro, V. Giovannetti, S. Guha, S. Lloyd, L. Maccone, and B. J. Yen, "Capacity of bosonic communications," in *Proc. 7th Int. Conf. Quantum Commun., Meas. Comput.*, S. M. Barnett, E. Anderson, J. Jeffers, P. Öhberg, and O. Hirota, Eds. New York: Amer. Inst. Phys., 2004, pp. 15–20.
- [34] J. W. Goodman, *Introduction to Fourier Optics*. New York: McGraw-Hill, 1968, ch. 4, 5, 8.
- [35] R. G. Gallager, *Information Theory and Reliable Communication*. New York: Wiley, 1968, ch. 8.
- [36] D. Slepian, "Prolate spheroidal wave functions, Fourier analysis and uncertainty—IV: Extension to many dimensions; generalized prolate spheroidal functions," *Bell Syst. Tech. J.*, vol. 43, pp. 3009–3057, Nov. 1964.
- [37] H. P. Yuen, "Two-photon coherent states of the radiation field," *Phys. Rev. A*, vol. 13, no. 6, pp. 2226–2243, Jun. 1976.
- [38] L.-A. Wu, M. Xiao, and H. J. Kimble, "Squeezed states from an optical parametric amplifier," *J. Opt. Soc. Amer. B*, vol. 4, no. 10, pp. 1465–1475, Oct. 1987.
- [39] J. H. Shapiro, H. P. Yuen, and J. A. Machado Mata, "Optical communication with two-photon coherent states—Part II: Photoemissive detection and structured receiver performance," *IEEE Trans. Inf. Theory*, vol. IT-25, no. 2, pp. 179–192, Mar. 1979.
- [40] C. M. Caves, "Quantum mechanical noise in an interferometer," *Phys. Rev. D*, vol. 23, no. 8, pp. 1693–1708, Apr. 1981.
- [41] J. H. Shapiro and K.-X. Sun, "Semiclassical versus quantum behavior in fourth-order interference," *J. Opt. Soc. Amer. B*, vol. 11, no. 6, pp. 1130–1141, Jun. 1994.
- [42] B. I. Erkmen and J. H. Shapiro, "Optical coherence theory for phase-sensitive light," *Proc. SPIE*, vol. 6305, pp. 6305G-1–6305G-12, 2006.
- [43] H. L. Van Trees, *Detection, Estimation, and Modulation Theory, Part I*. New York: Wiley, 1968, p. 229.

- [44] D. L. Snyder, *Random Point Processes*. New York: Wiley, 1975, ch. 2.
- [45] L. Mandel and E. Wolf, *Optical Coherence and Quantum Optics*. Cambridge, MA: Cambridge Univ. Press, 1995, ch. 9.
- [46] W. B. Davenport and W. L. Root, *An Introduction to the Theory of Random Signals and Noise*. New York: McGraw-Hill, 1958, ch. 7.
- [47] H. P. Yuen and V. W. S. Chan, "Noise in homodyne and heterodyne detection," *Opt. Lett.*, vol. 8, no. 3, pp. 177–179, Mar. 1983 (errata, *Opt. Lett.*, vol. 8, no. 6, p. 345, Jun. 1983).
- [48] J. H. Shapiro, "Quantum noise and excess noise in optical homodyne and heterodyne receivers," *IEEE J. Quantum Electron.*, vol. QE-21, no. 3, pp. 237–250, Mar. 1985.
- [49] D. L. Snyder, *Random Point Processes*. New York: Wiley, 1975, ch. 4.
- [50] R. M. Gagliardi and S. Karp, *Optical Communications*. New York: Wiley, 1976, ch. 6.
- [51] P. L. Kelley and W. H. Kleiner, "Theory of electromagnetic field measurement and photoelectron counting," *Phys. Rev.*, vol. 136, no. 2A, pp. A316–A334, Oct. 1964.
- [52] S. D. Personick, "An image-band interpretation of optical heterodyne noise," *Bell Syst. Tech. J.*, vol. 16, no. 1, pp. 625–628, Jan. 1971.
- [53] J. H. Shapiro and S. S. Wagner, "Phase and amplitude uncertainties in heterodyne detection," *IEEE J. Quantum Electron.*, vol. QE-20, no. 7, pp. 803–813, Jul. 1984.
- [54] M. B. Nasr, B. E. A. Saleh, A. V. Sergienko, and M. C. Teich, "Demonstration of dispersion-canceled quantum-optical coherence tomography," *Phys. Rev. Lett.*, vol. 91, no. 8, pp. 083601-1–083601-4, Aug. 2003.
- [55] T. B. Pittman, Y. H. Shih, D. V. Strekalov, and A. V. Sergienko, "Optical imaging by means of two-photon quantum entanglement," *Phys. Rev. A*, vol. 52, no. 5, pp. R3429–R3432, Nov. 1995.
- [56] V. Giovannetti, L. Maccone, J. H. Shapiro, and F. N. C. Wong, "Generating entangled two-photon states with coincident frequencies," *Phys. Rev. Lett.*, vol. 88, no. 18, pp. 183602-1–183602-4, May 2002.
- [57] M. Fiorentino, G. Messin, C. E. Kuklewicz, F. N. C. Wong, and J. H. Shapiro, "Generation of ultrabright tunable polarization entanglement without spatial, spectral, or temporal constraints," *Phys. Rev. A*, vol. 69, no. 4, pp. 041801(R)-1–041801(R)-4, Apr. 2004.
- [58] C. K. Law, I. A. Walmsley, and J. H. Eberly, "Continuous frequency entanglement: Effective finite Hilbert space and entropy control," *Phys. Rev. Lett.*, vol. 84, no. 23, pp. 5304–5307, Jun. 2000.
- [59] J. S. Bell, "On the problem of hidden variables in quantum mechanics," *Rev. Mod. Phys.*, vol. 38, no. 3, pp. 447–452, Jul. 1966.
- [60] P. Pearle, "Hidden variable examples based upon data rejection," *Phys. Rev. D*, vol. 2, no. 8, pp. 1418–1425, Oct. 1970.
- [61] A. Zeilinger, "Testing Bell's inequalities with periodic switching," *Phys. Lett. A*, vol. 118, no. 1, pp. 1–2, Sep. 1986.
- [62] C. E. Shannon, "A mathematical theory of communication, Part I," *Bell Syst. Tech. J.*, vol. 27, pp. 379–423, Jul. 1948.
- [63] C. E. Shannon, "A mathematical theory of communication, Part II," *Bell Syst. Tech. J.*, vol. 27, pp. 623–656, Oct. 1948.
- [64] T. M. Cover and J. A. Thomas, *Elements of Information Theory*. New York: Wiley, 1991, ch. 8, 10.
- [65] A. S. Holevo, "The capacity of a quantum channel with general signal states," *IEEE Trans. Inf. Theory*, vol. 44, no. 1, pp. 269–273, Jan. 1998.
- [66] P. Hausladen, R. Jozsa, B. Schumacher, M. Westmoreland, and W. K. Wootters, "Classical information capacity of a quantum channel," *Phys. Rev. A*, vol. 54, no. 3, pp. 1869–1876, Sep. 1996.
- [67] B. Schumacher and M. D. Westmoreland, "Sending classical information via noisy quantum channels," *Phys. Rev. A*, vol. 56, no. 1, pp. 131–138, Jul. 1997.
- [68] M. A. Nielsen and I. L. Chuang, *Quantum Computation and Quantum Information*. Cambridge, MA: Cambridge Univ. Press, 2000, sec. 8.2.4.
- [69] H. P. Yuen and M. Ozawa, "Ultimate information carrying limit of quantum systems," *Phys. Rev. Lett.*, vol. 70, no. 4, pp. 363–366, Jan. 1993.
- [70] A. Martinez, "Spectral efficiency of optical direct detection," *J. Opt. Soc. Amer. B*, vol. 24, no. 4, pp. 739–749, Apr. 2007.
- [71] A. Lapidoth and S. M. Moser, "On the capacity of the discrete-time Poisson channel," *IEEE Trans. Inf. Theory*, vol. 55, no. 1, pp. 303–322, Jan. 2009.
- [72] A. Lapidoth, J. H. Shapiro, V. Venkatesan, and L. Wang, "The Poisson channel at low input powers," in *Proc. 25th IEEE Convention Electr. Electron. Eng. Israel (IEEEI)*, Eilat, Israel, Dec. 2008, pp. 654–658.
- [73] N. S. Kopeika and J. Bordogna, "Background noise in optical communication systems," *Proc. IEEE*, vol. 58, no. 10, pp. 1571–1577, Oct. 1970.
- [74] J. H. Shapiro, S. Guha, and B. I. Erkmen, "Ultimate capacity of free-space optical communications," *J. Opt. Netw.*, vol. 4, no. 8, pp. 501–516, Aug. 2005.
- [75] V. Giovannetti, S. Guha, S. Lloyd, L. Maccone, J. H. Shapiro, B. J. Yen, and H. P. Yuen, "Classical capacity of free-space optical communications," in *Quantum Information, Statistics, and Probability*, O. Hirota, Ed. Princeton, NJ: Rinton, 2004, pp. 90–101.
- [76] B. I. Erkmen and J. H. Shapiro, "Unified theory of ghost imaging with Gaussian-state light," *Phys. Rev. A*, vol. 77, no. 4, pp. 043809-1–043809-13, Apr. 2008.
- [77] B. I. Erkmen and J. H. Shapiro, "Signal-to-noise ratio of Gaussian-state ghost imaging," *Phys. Rev. A*, vol. 79, no. 2, pp. 023833-1–023833-11, Feb. 2009.
- [78] V. Giovannetti, S. Lloyd, L. Maccone, and P. W. Shor, "Entanglement assisted capacity of the broadband lossy channel," *Phys. Rev. Lett.*, vol. 91, no. 4, pp. 047901-1–047901-4, Jul. 2003.
- [79] M. M. Wolf, D. Pérez-García, and G. Giedke, "Quantum capacities of bosonic channels," *Phys. Rev. Lett.*, vol. 98, no. 13, pp. 130501-1–130501-4, Mar. 2007.
- [80] B. J. Yen and J. H. Shapiro, "Multiple-access bosonic communications," *Phys. Rev. A*, vol. 72, no. 6, pp. 062312-1–062312-10, Dec. 2005.
- [81] S. Guha, J. H. Shapiro, and B. I. Erkmen, "Classical capacity of bosonic broadcast communication and a minimum output entropy conjecture," *Phys. Rev. A*, vol. 76, no. 3, pp. 032303-1–032303-12, Sep. 2007.
- [82] S. Lloyd, V. Giovannetti, L. Maccone, N. J. Cerf, S. Guha, R. García-Patrón, S. Mitter, S. Pirandola, M. B. Ruskai, J. H. Shapiro, and H. Yuan, "Proof of the bosonic minimum output entropy conjecture," arXiv:0906.2758 [quant-ph], Jun. 2009.
- [83] S. Lloyd, V. Giovannetti, L. Maccone, S. Pirandola, and R. García-Patrón, "Minimum output entropy of Gaussian channels," arXiv:0906.2762 [quant-ph], Jun. 2009.



Jeffrey H. Shapiro (S'67–M'70–SM'84–F'95) received the S.B., S.M., E.E., and Ph.D. degrees in electrical engineering from Massachusetts Institute of Technology (MIT), Cambridge, in 1967, 1968, 1969, and 1970, respectively.

As a graduate student, he was a National Science Foundation Fellow, a Teaching Assistant, and a Fannie and John Hertz Foundation Fellow. His doctoral research was a theoretical study of adaptive techniques for improved optical communication through atmospheric turbulence. From 1970 to 1973, he was

an Assistant Professor of electrical sciences and applied physics at Case Western Reserve University, Cleveland, OH. From 1973 to 1985, he was an Associate Professor of electrical engineering at MIT, where he was promoted to a Professor of electrical engineering in 1985, was the Associate Department Head of the Department of Electrical Engineering and Computer Science from 1989 to 1999, and has been the Director of the Research Laboratory of Electronics (RLE) since 2001. In 1999, he became the Julius A. Stratton Professor of Electrical Engineering. His current research interests center on the application of communication theory to optical systems. He is best known for his work on the generation, detection, and application of squeezed-state light beams, but he has also published extensively in the areas of atmospheric optical communication, coherent laser radar, and quantum information science.

Prof. Shapiro is a Fellow of the Optical Society of America, the American Physical Society, and the Institute of Physics. He is a member of the International Society for Optical Engineering. In 2008, he was a corecipient of the Quantum Electronics Award from the IEEE Photonics Society (formerly known as IEEE Lasers and Electro-Optics Society), and also received the Quantum Communication Award for Theoretical Research from Tamagawa University, Tokyo, Japan. He has been an Associate Editor of the IEEE TRANSACTIONS ON INFORMATION THEORY and the *Journal of the Optical Society of America*. He was the Principal Organizer of the Sixth International Conference on Quantum Communication, Measurement and Computing (QCMC), 2002. He is currently the Chair of the Steering Committee for the International Conferences on Quantum Communication, Measurement and Computing, the Co-Director of the W. M. Keck Foundation Center for Extreme Quantum Information Theory (xQIT), and the Co-Director of the Interdisciplinary Quantum Information Science and Engineering (iQIUSE) Program.